Copy
RM L57E16a

NACA

RESEARCH MEMORANDUM

AERODYNAMIC CHARACTERISTICS OF A SPOILER-SLOT-DEFLECTOR CONTROL ON A 45° SWEPTBACK WING AT MACH NUMBERS OF 1.61 AND 2.01

By Douglas R. Lord and Robert Moring

Langley Aeronautical Laboratory
Langley Field, Va.

NATIONAL ADVISORY COMMITTEE
FOR AERONAUTICS

WASHINGTON
July 17, 1957

NATIONAL ADVISORY COMMITTEE FOR AERONAUTICS

RESEARCH MEMORANDUM

AERODYNAMIC CHARACTERISTICS OF A SPOILER-SLOT-DEFLECTOR CONTROL ON A 45° SWEPTBACK WING AT MACH NUMBERS OF 1.61 AND 2.01

By Douglas R. Lord and Robert Moring

SUMMARY

An investigation has been made in the Langley 4- by 4-foot supersonic pressure tunnel at Mach numbers of 1.61 and 2.01 to determine the aerodynamic characteristics of a spoiler-slot-deflector control on a 45° sweptback wing having an aspect ratio of 3.5, a taper ratio of 0.3, and an NACA 65A005 airfoil section. The model was equipped with a 15-percent-chord spoiler-slot-deflector extending from 13 to 78 percent of the wing semispan. The spoiler and deflector were hinged along the 60- and 75-percent-chord lines, respectively. Tests were made at a Reynolds number of 3.0×10^6 (based on the mean aerodynamic chord of the wing) and covered ranges of angles of attack from -3° to 15°, spoiler projections from 0 to 8.0 percent chord, and deflector projections from 0 to 7.6 percent chord.

The test results indicated that the spoiler-alone configuration lost very little effectiveness at angles of attack up to 15°, however, projecting the deflector caused large increases in effectiveness at the high angles of attack. Ratios of deflector projection to spoiler projection from 0.5 to 1.0 produced the maximum control effectiveness and ratios near 0.5 produced the minimum total hinge moments.

INTRODUCTION

Considerable interest is being manifested in spoiler-type controls for use in obtaining lateral control on high-speed aircraft. These controls are desirable because of their good effectiveness through the transonic speed range, low hinge moments, and low aeroelastic effects as compared to conventional trailing-edge ailerons. At high angles of attack, spoiler controls tend to lose their effectiveness; however, a slot behind the spoiler and a lower surface deflector have been found to improve greatly the effectiveness at angles of attack in the subsonic

and transonic speed ranges. (See refs. 1 to 14.) The results to date are primarily from wind-tunnel tests; however, successful flight tests of a spoiler-slot-deflector control have been made at high subsonic speeds by North American Aviation, Inc., on a full-scale airplane. The purpose of this report is to present the results of some supersonic wind-tunnel tests of a spoiler-slot-deflector configuration and to determine the most suitable ratios of deflector projection to spoiler projection for maximum effectiveness and minimum hinge moments.

The semispan wing model was tested in the presence of a half-fuselage at angles of attack from -3° to 15°. The spoiler and deflector were projected independently through projection ranges from 0 to 8.0 percent chord. The tests were conducted at Mach numbers of 1.61 and 2.01 for a Reynolds number of 3.0×10^6, based on the wing mean aerodynamic chord of 10.65 inches.

SYMBOLS

C_L semispan wing lift coefficient, $\frac{\text{Lift}}{qS}$

C_D semispan wing drag coefficient, $\frac{\text{Drag}}{qS}$

C_m semispan wing pitching-moment coefficient referred to $0.25\bar{c}$, $\frac{\text{Pitching moment}}{qS\bar{c}}$

$C_{l,\text{gross}}$ semispan wing rolling-moment coefficient, $\frac{\text{Rolling moment}}{2qSb}$

C_l incremental rolling-moment coefficient produced by control

C_h hinge-moment coefficient about control hinge axis, $\frac{\text{Hinge moment}}{2qQ}$, positive hinge moment is a closing moment

$C_{h,t}$ total hinge-moment coefficient, $C_{h,s}\frac{Q_s}{Q_t} + \frac{\partial\delta_d}{\partial\delta_s} C_{h,d}\frac{Q_d}{Q_t}$

$\frac{b}{2}$ wing semispan

c local wing chord

$\bar{c}$	wing mean aerodynamic chord
M	stream Mach number
q	stream dynamic pressure
Q	area moment of control about its hinge line
S	semispan wing area
α	wing angle of attack
δ	control projection perpendicular to the wing surface (negative for spoiler trailing edge above and deflector trailing edge below wing surface)
Δ	prefix indicating increment due to control

Subscripts:

s	spoiler
d	deflector
t	total

APPARATUS

Wind Tunnel

This investigation was conducted in the Langley 4- by 4-foot supersonic pressure tunnel, which is a rectangular, closed-throat, single-return type of wind tunnel with provisions for the control of the pressure, temperature, and humidity of the enclosed air. Flexible nozzle walls were adjusted to give the desired test section Mach numbers of 1.61 and 2.01. During the tests, the dewpoint was kept below -20° F at atmospheric pressure so that the effects of water condensation in the supersonic nozzle were negligible.

Model and Model Mounting

The model used in these tests consisted of a semispan wing and a half-fuselage as shown in figure 1. The wing was made of steel and had 45° sweepback of the quarter-chord line, an aspect ratio of 3.5, a taper ratio of 0.3, a root chord of 14.95 inches, a tip chord of 4.48 inches,

and a semispan of 17.00 inches. The wing had NACA 65A005 airfoil sections parallel to the air stream and was equipped with an inboard 65-percent-semispan, 15-percent-wing chord spoiler-slot-deflector. The spoiler and deflector were hinged along the 60-percent- and 75-percent-chord lines, respectively. (See fig. 1.)

The fuselage was made of steel and aluminum. It had a fineness-ratio-2.5 ogival nose followed by a cylindrical center portion and a boattailed afterbody with a base diameter of 50 percent of the maximum body diameter. (See fig. 1.)

The semispan sweptback wing was mounted on a sidewall balance which was located in a turntable of a boundary-layer bypass plate as shown in figure 2. The bypass plate was located about 10 inches from the tunnel sidewall. The half-fuselage was mounted on the turntable independently of the wing and balance.

TESTS

The forces and moments on the wing in the presence of the body were measured by a four-component strain-gage balance. The spoiler and deflector hinge moments were measured by strain gages mounted on the linkage which connected the control drive motors to the control shafts. These strain gages measured the moments about the shafts.

The model angle of attack was changed by a motor drive located outside the tunnel which rotated the turntable in the bypass plate on which the model was mounted. The angle of attack was measured by an electrical slide-wire position indicator located on the backside of the turntable in the bypass plate. Spoiler and deflector projections were changed by two remote-controlled electrical motors mounted in the fuselage and geared to rotate the control shafts. The angles of the control shafts were measured by two electrical slide-wire control-position indicators located inside the fuselage. Calibrations of the control projections in terms of the control shaft angles were made to enable the test to be made at even-percent-chord projections.

The wing angle-of-attack range was from -3° to 15° at increments of 3°. The spoiler projection range was from 0 to -8.0 percent wing chord with a range of deflector projection from zero to a projection approximately equal to that of the spoiler at each spoiler projection. In addition, at a spoiler setting of 0, the deflector was tested at projections from 0 to -7.6 percent chord.

The tests were made at tunnel stagnation pressures of 12.0 and 14.0 pounds per square inch at Mach numbers of 1.61 and 2.01,

respectively, corresponding to a Reynolds number based on the wing mean aerodynamic chord of 3.0×10^6. In order to insure a turbulent boundary layer over the wing during the test, 1/8-inch-wide strips of No. 60 carborundum grains were attached to the wing upper and lower surfaces at a distance of 3/4 inch from the leading edge. These strips extended from the fuselage to the semispan wing tip.

PRECISION OF DATA

The mean Mach numbers in the region occupied by the model were estimated from calibration to be 1.61 and 2.01 with local variations smaller than ±0.02. There was no evidence of significant flow angularity. The estimated accuracy of other pertinent quantities is as follows:

α, deg	±0.05
δ_s, percent chord	±0.2
δ_d, percent chord	±0.2
C_L	±0.005
C_D	±0.001
C_m	±0.002
$C_{l,gross}$	±0.001
$C_{h,s}$	±0.01
$C_{h,d}$	±0.02

RESULTS AND DISCUSSION

Basic Wing Characteristics

The variations of wing lift, drag, pitching moment, and gross rolling-moment coefficients with angle of attack for the basic wing configuration with undeflected controls are shown in figure 3. These variations are presented in order to illustrate the magnitude of the coefficients at the two Mach numbers and because the ensuing analysis of the control characteristics relies on the incremental coefficients due to deflecting the controls.

In general the curves of the various wing coefficients with angle of attack (fig. 3) are smooth and the effect of increasing the Mach number from 1.61 to 2.01 is to decrease the slopes of the curves. Some inaccuracies are evident in the data at $\alpha = 0^\circ$ where the lift, pitching-moment, and rolling-moment coefficients are not always zero and the drag coefficients are somewhat higher at $M = 2.01$ than at $M = 1.61$, contrary to what might be expected. One possible explanation for the drag

difference could be that the transition strips were made too thick for the M = 2 tests. The faired values taken from the curves of figure 3, however, were subtracted from the measured values with the controls deflected in order to obtain the incremental coefficients due to control deflection.

Control Effectiveness and Drag

The basic plots of the incremental wing lift, drag, pitching-moment, and rolling-moment coefficients due to deflecting the spoiler-slot-deflector control are presented in figures 4 and 5. The various coefficients are plotted against deflector projection for constant spoiler projection at a given wing angle of attack.

At low angles of attack there is very little change in the effectiveness or drag due to increasing the Mach number from 1.61 to 2.01. As the angle of attack is increased toward 15°, however, the effect of Mach number becomes quite significant. At low angles of attack, increasing the deflector projection generally causes small changes in the wing lift, pitching-moment, or rolling-moment coefficients; but at the higher angles of attack, the effect of the deflector is very beneficial. This is in agreement with effects previously shown in references 3, 4, and 5 which seem to indicate that the deflector becomes less effective at the low angles of attack as the wing sweep or Mach number is increased. On the other hand, the deflector causes sizeable drag increases at the low angles of attack (fig. 4); whereas, at high angles of attack when the spoiler is open, the deflector causes negligible changes in drag. This trend is also in agreement with the drag characteristics shown in reference 3.

In order to demonstrate more vividly the effect of angle of attack on the control effectiveness and drag characteristics, the incremental coefficients from figures 4 and 5 have been cross-plotted against angle of attack in figures 6 and 7 for constant spoiler projections and at ratios of deflector projection to spoiler projection of 0, 0.5, and 1.0. It should be evident that a projection ratio of zero corresponds to a spoiler-alone configuration.

Perhaps the most remarkable effect shown in figures 6(a) and 7(a) is the small loss in control effectiveness for this particular spoiler-alone configuration with increasing angle of attack. Similar variations have been shown in references 4 and 5 for M = 1.20 with somewhat greater loss for the unswept wing configuration than for the swept configuration. When the deflector was geared to open one-half as (figs. 6(b) and 7(b)) or as much as (figs. 6(c) and 7(c)) the spoiler, the control effectiveness increased considerably with angle of attack. This increased effectiveness is much larger at M = 1.61 than at M = 2.01. In considering the drag due to the controls, it can be seen from figure 6 that increasing

the projection ratio δ_d/δ_s generally increases the drag throughout most of the angle-of-attack range; however, the drag increment at the high angles of attack remains negligible.

Since the most practical application for the spoiler-slot-deflector type of control at the present time is for use as a lateral-control device, a more detailed analysis of the rolling-moment effectiveness for this control is shown in figure 8 where rolling-moment coefficient is plotted against the ratio of deflector projection to spoiler projection at four angles of attack and three spoiler projections.

The variations shown in figure 8 indicate that for the spoiler projections required to obtain appreciable rolling moment, the ratio of deflector projection to spoiler projection for maximum rolling moment increases with angle of attack. This increasing trend with angle of attack has been demonstrated previously at subsonic speeds in references 3 and 11. At $M = 1.61$ a projection ratio of 0.5 is the optimum at $\alpha = 0^\circ$, whereas projection ratios of the order of 0.8 to 1.0 are beneficial at the highest angles of attack. At $M = 2.01$ a projection ratio of 0.7 is the optimum at $\alpha = 0^\circ$ and again projection ratios of 0.8 to 1.0 are beneficial at the highest angles of attack.

Control Hinge Moments

The basic variations of spoiler and deflector hinge-moment coefficients with deflector projection for constant spoiler projections at a given angle of attack are presented in figure 9. In general the variations are very similar to those shown at high subsonic speeds in reference 13. The effect of increasing the Mach number from 1.61 to 2.01 as shown in figure 9 is small on both the spoiler and deflector hinge-moment coefficient. Increasing the deflector projection for a constant spoiler projection decreases the spoiler hinge-moment coefficient. The rate at which the deflector decreases the spoiler hinge-moment coefficient is greater at the larger angles of attack. With the deflector projection fixed, increasing the spoiler projection increased the spoiler hinge-moment coefficient (made more positive). The maximum increases were obtained in the middle of the deflector projection range at large angles of attack.

At low angles of attack, the deflector hinge-moment coefficients increase rapidly (become more negative) with increasing deflector projection. At the higher angles of attack, the deflector hinge-moment coefficients first became more positive as the deflector projection increases until a critical point is reached beyond which the deflector hinge-moment coefficients abruptly became negative. The critical deflector projection at which this reversal occurs increases with angle of

attack from -0.25 percent chord at $\alpha = 3^\circ$ to -1.0 percent chord at $\alpha = 15^\circ$. Varying the spoiler projection at a given deflector projection causes relatively small changes in the deflector hinge-moment coefficient.

The changes in spoiler and deflector hinge-moment coefficients with angle of attack are more clearly shown in figure 10 where the data from figure 9 have been cross-plotted against angle of attack for constant spoiler projections and ratios of deflector projection to spoiler projection of 0, 0.5, and 1.0. For the spoiler-alone configuration (fig. 10(a)), the spoiler hinge-moment coefficients decreased and the effect of spoiler projection decreased as the angle of attack was increased. The deflector hinge-moment coefficients show little effect of either angle of attack or spoiler deflection for the spoiler-alone configuration as would be expected.

For the spoiler-slot-deflector configuration with ratios of deflector projection to spoiler projection of 0.5 (fig. 10(b)) and 1.0 (fig. 10(c)), the spoiler hinge-moment coefficients decreased with angle of attack, though the effect of spoiler projection remained relatively constant. The deflector hinge-moment coefficients for these same configurations exhibited large and sometimes erratic changes both with angle of attack and with spoiler deflection. For $\delta_d/\delta_s = 0.5$ the deflector hinge-moment coefficients tended to decrease (become more positive) with increasing angle of attack, whereas for $\delta_d/\delta_s = 1.0$ they tended to increase with increasing angle of attack.

Since the hinge moments produced by the spoiler and by the deflector generally are of opposite sign, it will be of interest to consider the total hinge-moment coefficients for a geared spoiler-slot-deflector configuration. In figure 11 the total hinge-moment coefficients are plotted against ratio of deflector projection to spoiler projection at four angles of attack and three spoiler projections. As the projection ratio is increased, the total hinge-moment coefficients change from positive to negative as the equation for determining the total hinge-moment coefficients is first dominated by the positive spoiler hinge moments and then by the negative deflector hinge moments. It appears from figure 11 that a projection ratio of 0.5 would be optimum for obtaining minimum total hinge moments throughout the angle of attack, spoiler projection, and Mach number ranges covered herein.

CONCLUSIONS

An investigation has been made at Mach numbers of 1.61 and 2.01 to determine the aerodynamic characteristics of a spoiler-slot-deflector control on a 45° sweptback wing. The results indicate the following conclusions:

1. The spoiler-alone configuration exhibited relatively small losses in effectiveness at angles of attack up to 15°.

2. At angles of attack above 0°, projecting the deflector caused large increases in spoiler effectiveness.

3. Ratios of deflector projection to spoiler projection from 0.5 to 1.0 produced the maximum control effectiveness throughout the angle-of-attack range and caused little drag penalty at angles of attack.

4. The total hinge-moment coefficients produced by the geared spoiler-slot-deflector control were smallest for a ratio of deflector projection to spoiler projection of about 0.5.

Langley Aeronautical Laboratory,
National Advisory Committee for Aeronautics,
Langley Field, Va., April 24, 1957.

REFERENCES

1. Wenzinger, Carl J., and Rogallo, Francis M.: Wind-Tunnel Investigation of Spoiler, Deflector, and Slot Lateral-Control Devices on Wings With Full-Span Split and Slotted Flaps. NACA Rep. 706, 1941.

2. Watson, James M.: Low-Speed Lateral-Control Investigation of a Flap-Type Spoiler Aileron With and Without a Deflector and Slot on a 6-Percent-Thick, Tapered, 45° Sweptback Wing of Aspect Ratio 4. NACA RM L52G10, 1952.

3. Vogler, Raymond D.: Wind-Tunnel Investigation at High Subsonic Speeds of a Spoiler-Slot-Deflector Combination on an NACA 65A006 Wing With Quarter-Chord Line Swept Back 32.6°. NACA RM L53D17, 1953.

4. Lowry, John G.: Data on Spoiler-Type Ailerons. NACA RM L53I24a, 1953.

5. Vogler, Raymond D.: Wind-Tunnel Investigation at Transonic Speeds of a Spoiler-Slot-Deflector Combination on an Unswept NACA 65A006 Wing. NACA RM L53J21, 1953.

6. Thompson, Robert F., and Taylor, Robert T.: Effect of a Wing Leading-Edge Flap and Chord-Extension on the High Subsonic Control Characteristics of a Spoiler-Slot-Deflector Control Located at Two Spanwise Positions. NACA RM L54I09, 1954.

7. Hammond, Alexander D.: Loads on Wings Due to Spoilers at Subsonic and Transonic Speeds. NACA RM L55E17a, 1955.

8. Hammond, Alexander D.: Low-Speed Pressure Distribution Investigation of a Spoiler and a Spoiler-Slot-Deflector on a 30° Sweptback Wing-Fuselage Model Having an Aspect Ratio of 3, a Taper Ratio of 0.5, and NACA 65A004 Airfoil Section. NACA RM L55I29, 1956.

9. Scallion, William I.: Full-Scale Wind-Tunnel Tests of a 35° Swept-Wing Fighter Airplane With a Spoiler-Slot-Deflector Lateral Control System. NACA RM L56D18, 1956.

10. West, F. E., Jr., Whitcomb, Charles F., and Schmeer, James W.: Investigation of Spoiler-Slot-Deflector Ailerons and Other Spoiler Ailerons on a 45° Sweptback-Wing—Fuselage Combination at Mach Numbers From 0.60 to 1.03. NACA RM L56F15, 1956.

11. Hammond, Alexander D.: Low-Speed Investigation of the Lateral-Control Characteristics of a Flap-Type Spoiler and a Spoiler-Slot-Deflector on a 30° Sweptback Wing-Fuselage Model Having an Aspect Ratio of 3, a Taper Ratio of 0.5, and NACA 65A004 Airfoil Section. NACA RM L56F18, 1956.

12. Hammond, Alexander D., and Huffman, Jarrett K.: A Low-Speed Investigation of a High-Lift Lateral-Control Device Consisting of a Spoiler-Slot-Deflector and a Trailing-Edge Flap on a Tapered 45° Sweptback Wing. NACA RM L56H31, 1956.

13. Hammond, Alexander D., and Brown, Albert E.: The Results of an Investigation at High Subsonic Speeds To Determine the Lateral-Control and Hinge-Moment Characteristics of a Spoiler-Slot-Deflector Configuration on a 35° Sweptback Wing. NACA RM L57C20, 1957.

14. O'Keefe, D., et al.: Low Speed Wind Tunnel Tests of a 0.20-Scale Simulated Model of the FJ-3 Airplane To Determine the General Stability and Control Characteristics With an Aileron Spoiler-Slot Deflector and With Under-Wing Fuel Tanks, Rocket Packages, and Pylons. Rep. No. NA-55-1235 (NAAL-313), North American Aviation, Inc., Nov. 16, 1955.

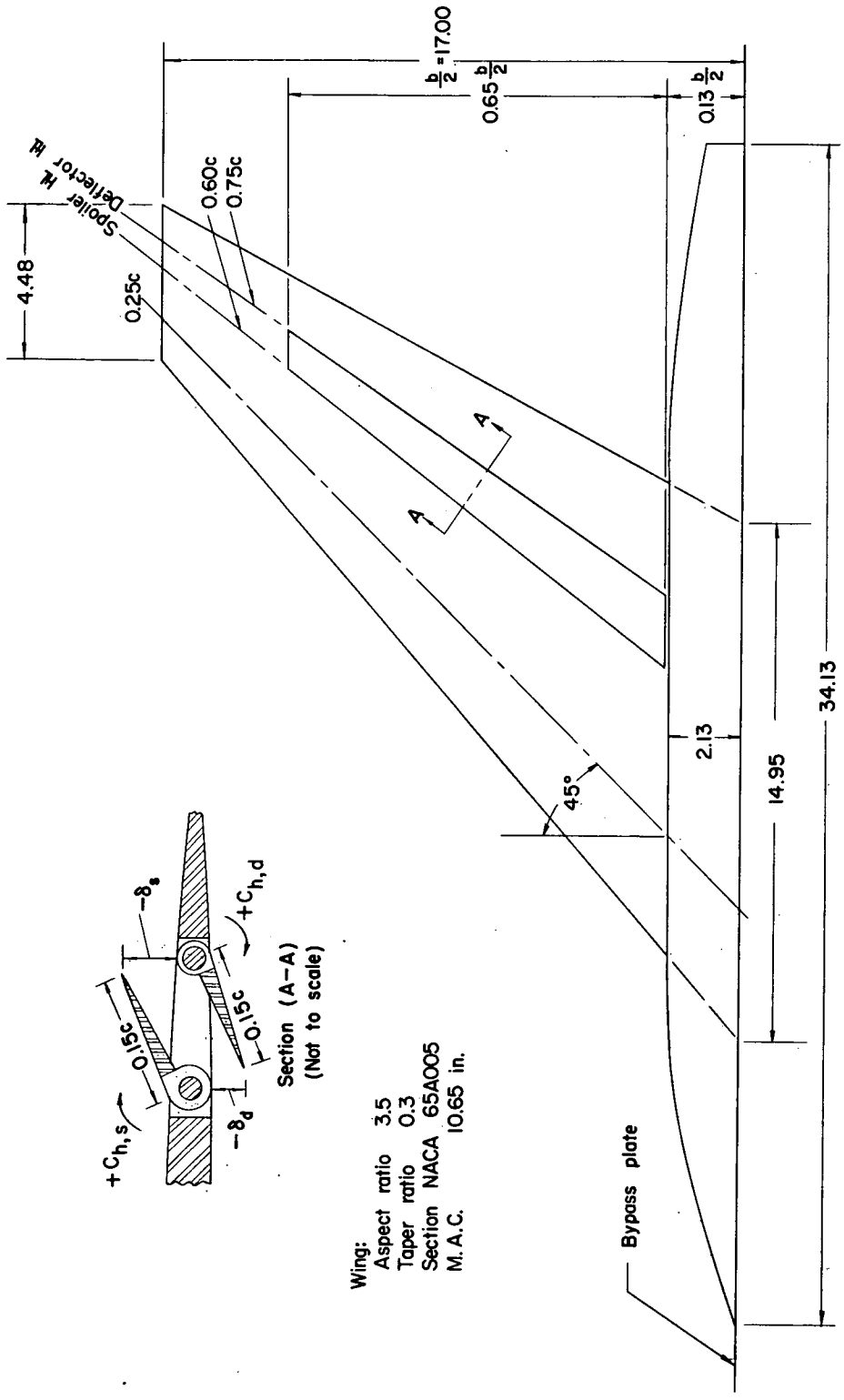

Figure 1.- Sketch of semispan wing-fuselage model. All dimensions are in inches.

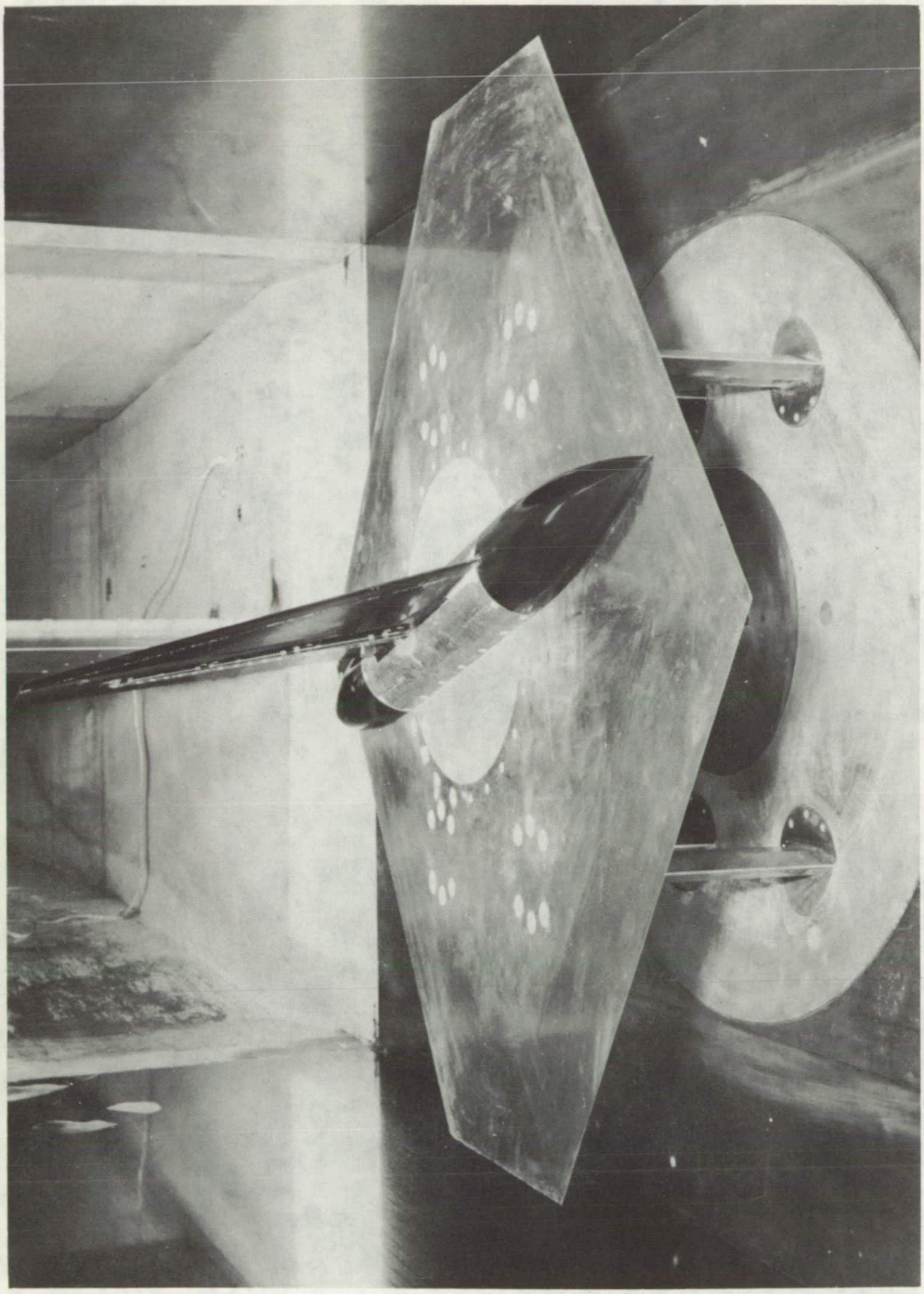

(a) Front three-quarter view. L-96391

Figure 2.- Model mounted on the boundary-layer bypass plate.

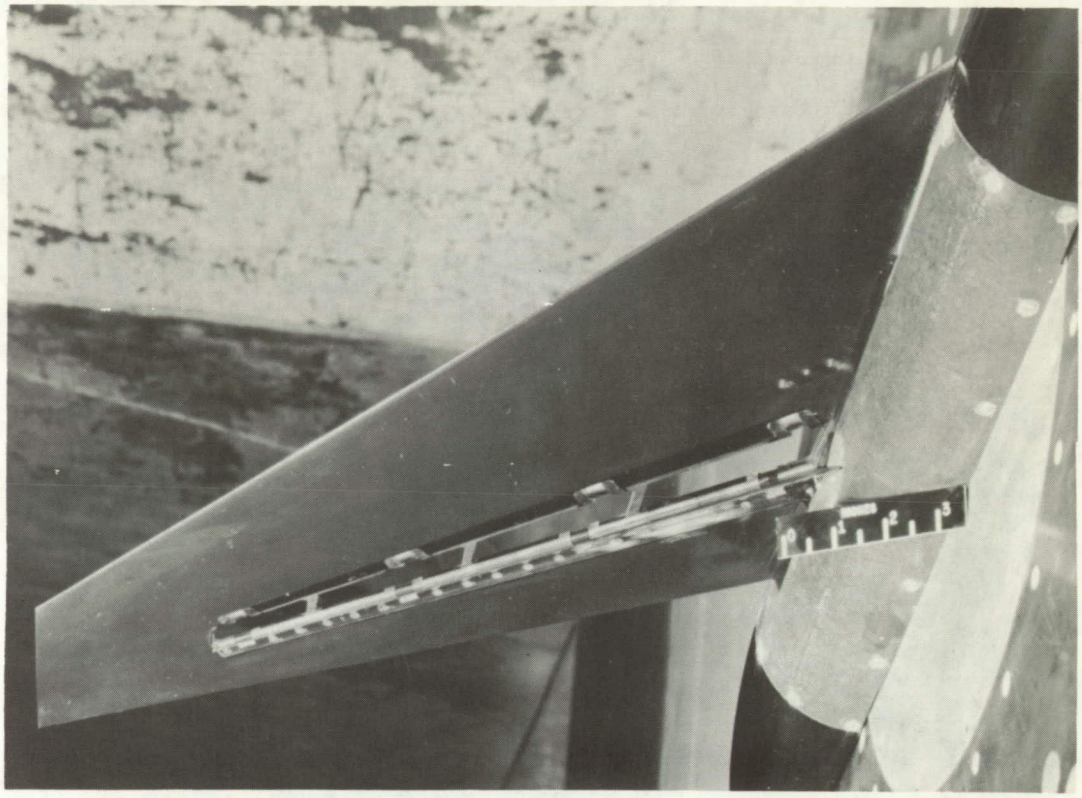

L-57-498

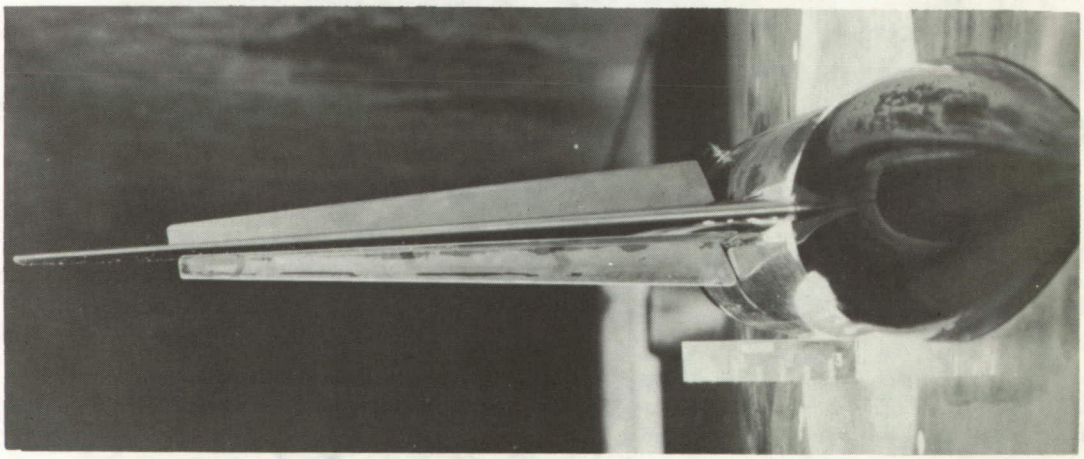

L-57-499

(b) Bottom and front views with spoiler and deflector controls open.

Figure 2.- Concluded.

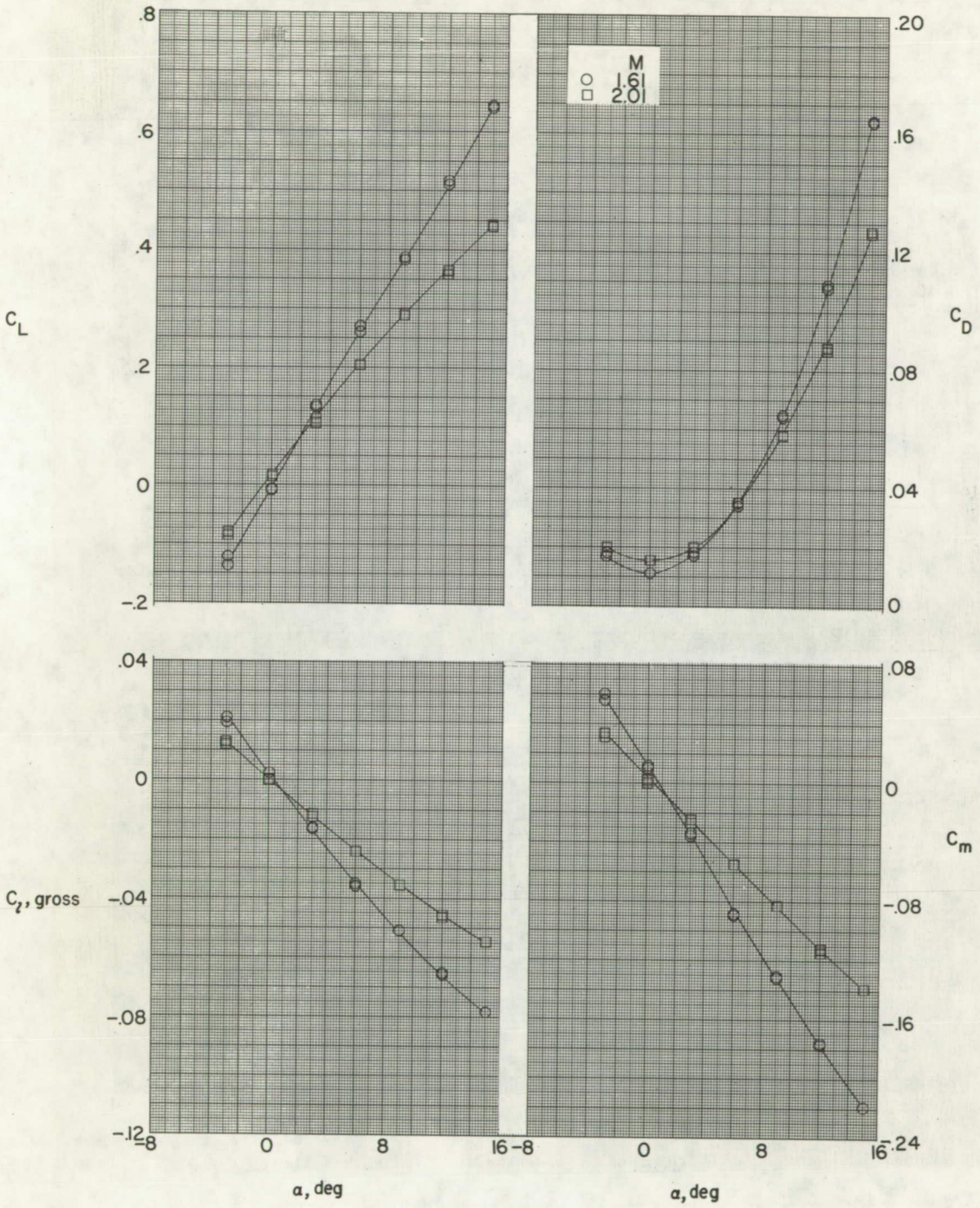

Figure 3.- Variation of wing lift, drag, pitching-moment, and gross rolling-moment coefficients with angle of attack. $\delta_s = 0$; $\delta_d = 0$.

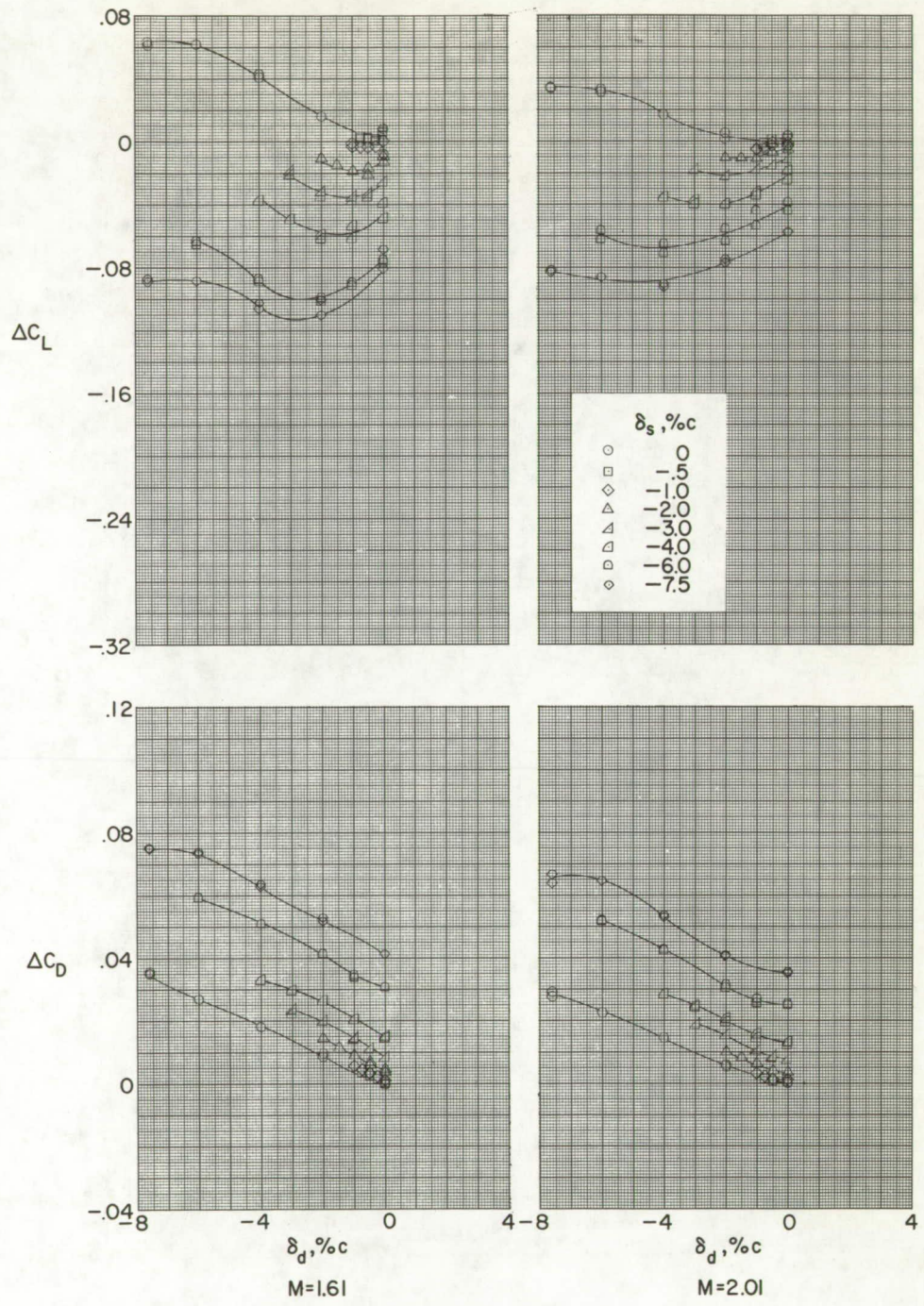

(a) $\alpha = -3^{\circ}$.

Figure 4.- Variation of incremental wing lift and drag coefficients with deflector projection.

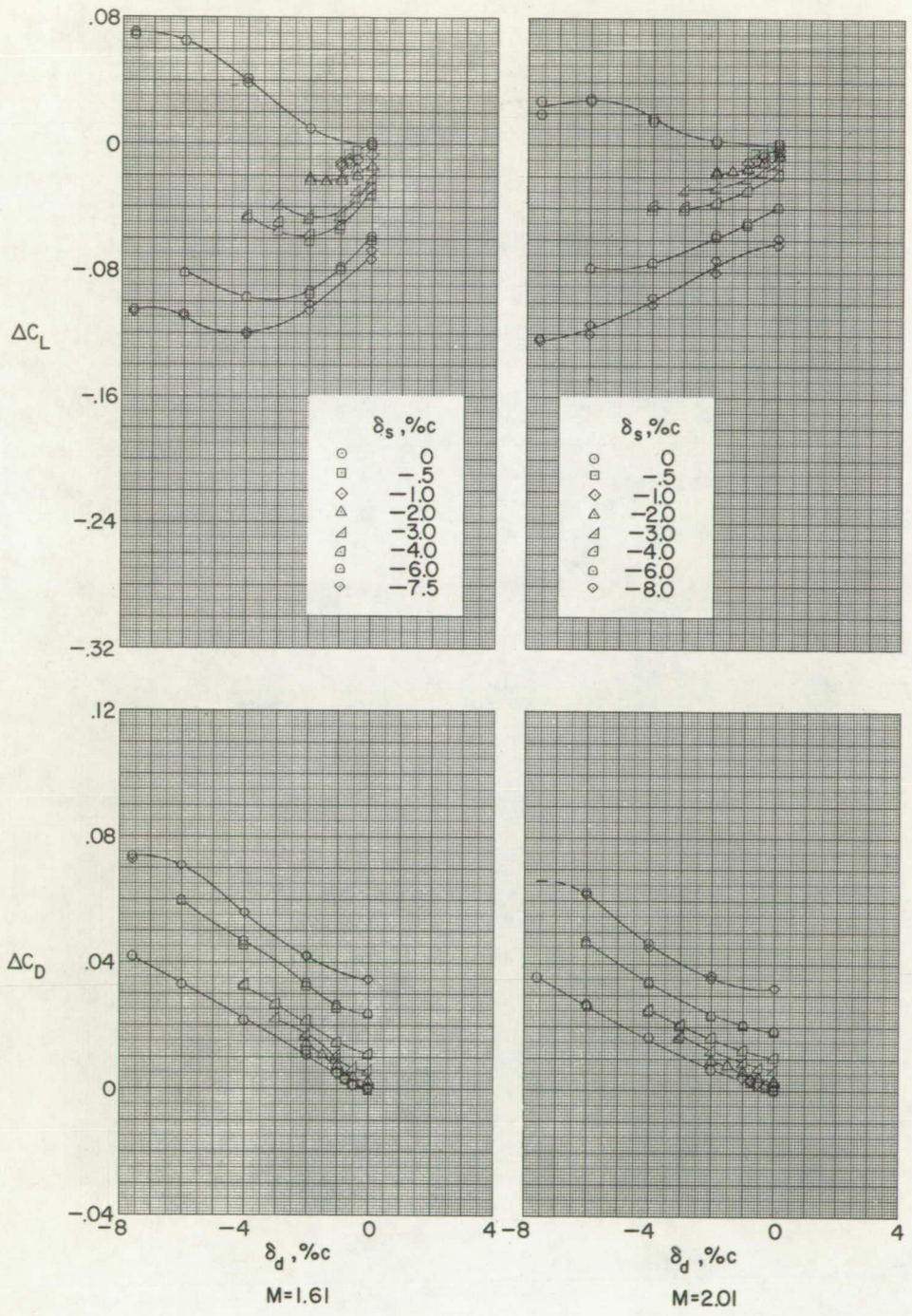

(b) $\alpha = 0^{\circ}$.

Figure 4.- Continued.

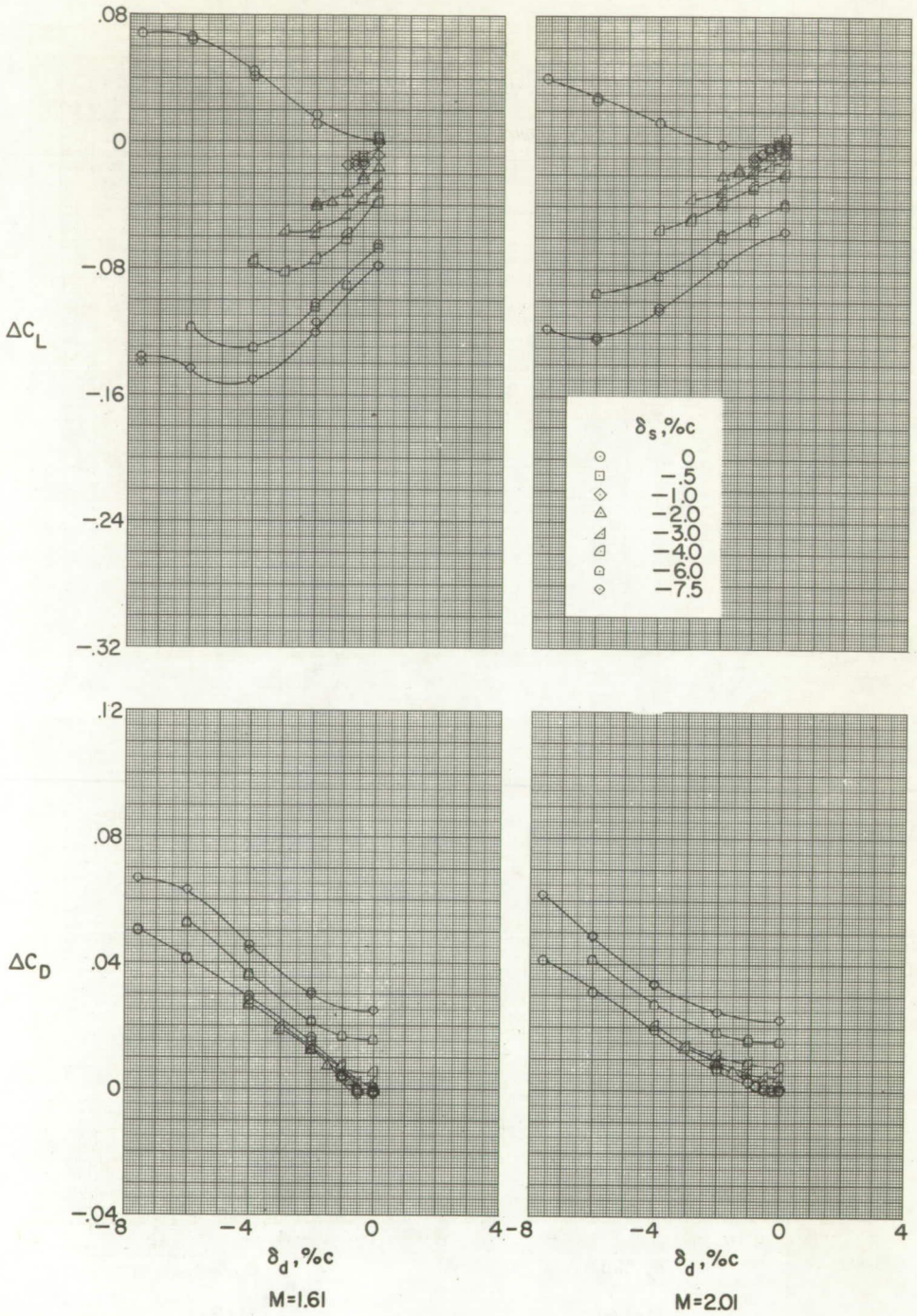

(c) $\alpha = 3^\circ$.

Figure 4.- Continued.

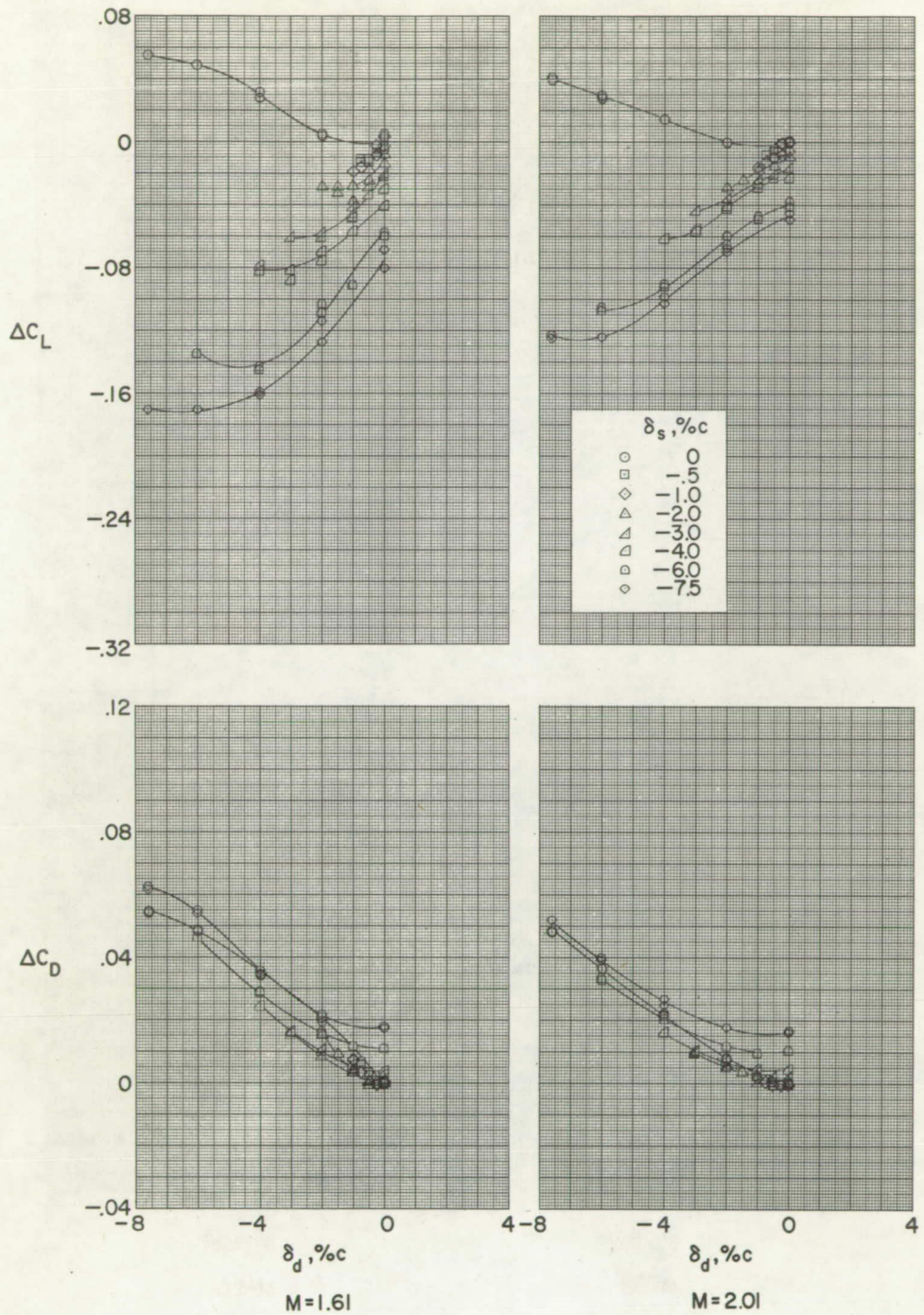

(d) $\alpha = 6^{\circ}$.

Figure 4.- Continued.

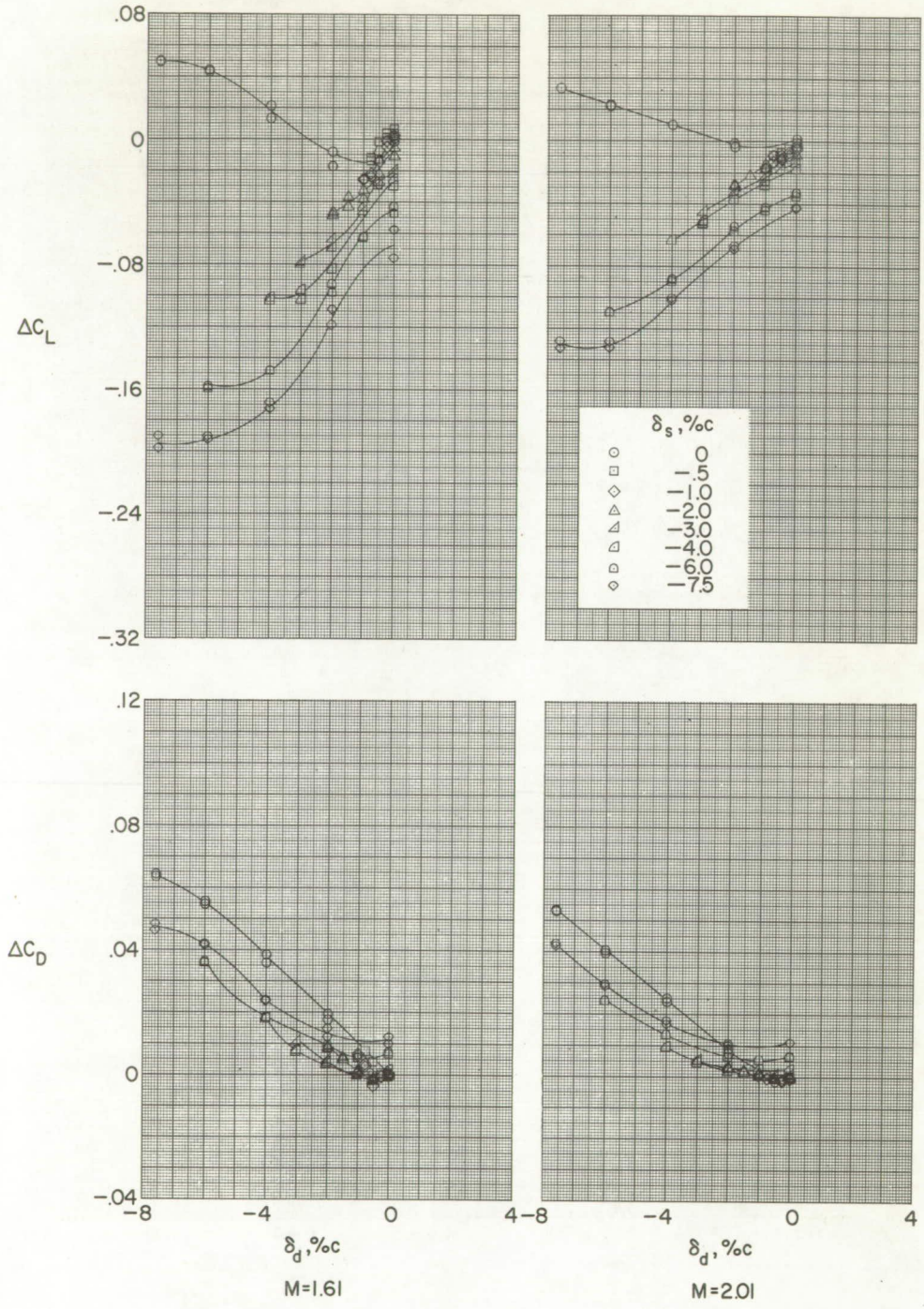

(e) $\alpha = 9^{\circ}$.

Figure 4.- Continued.

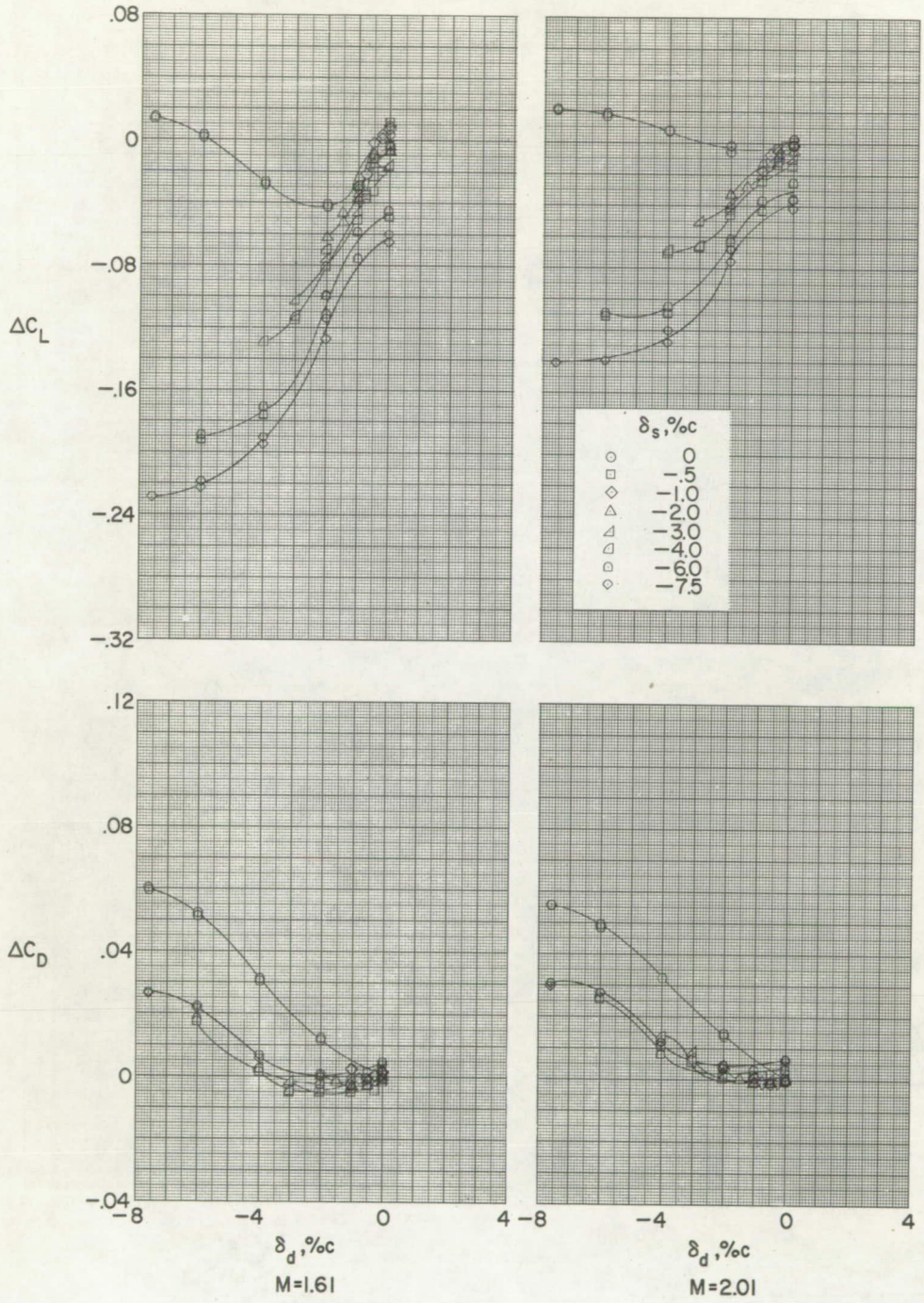

(f) $\alpha = 12^{\circ}$.

Figure 4.- Continued.

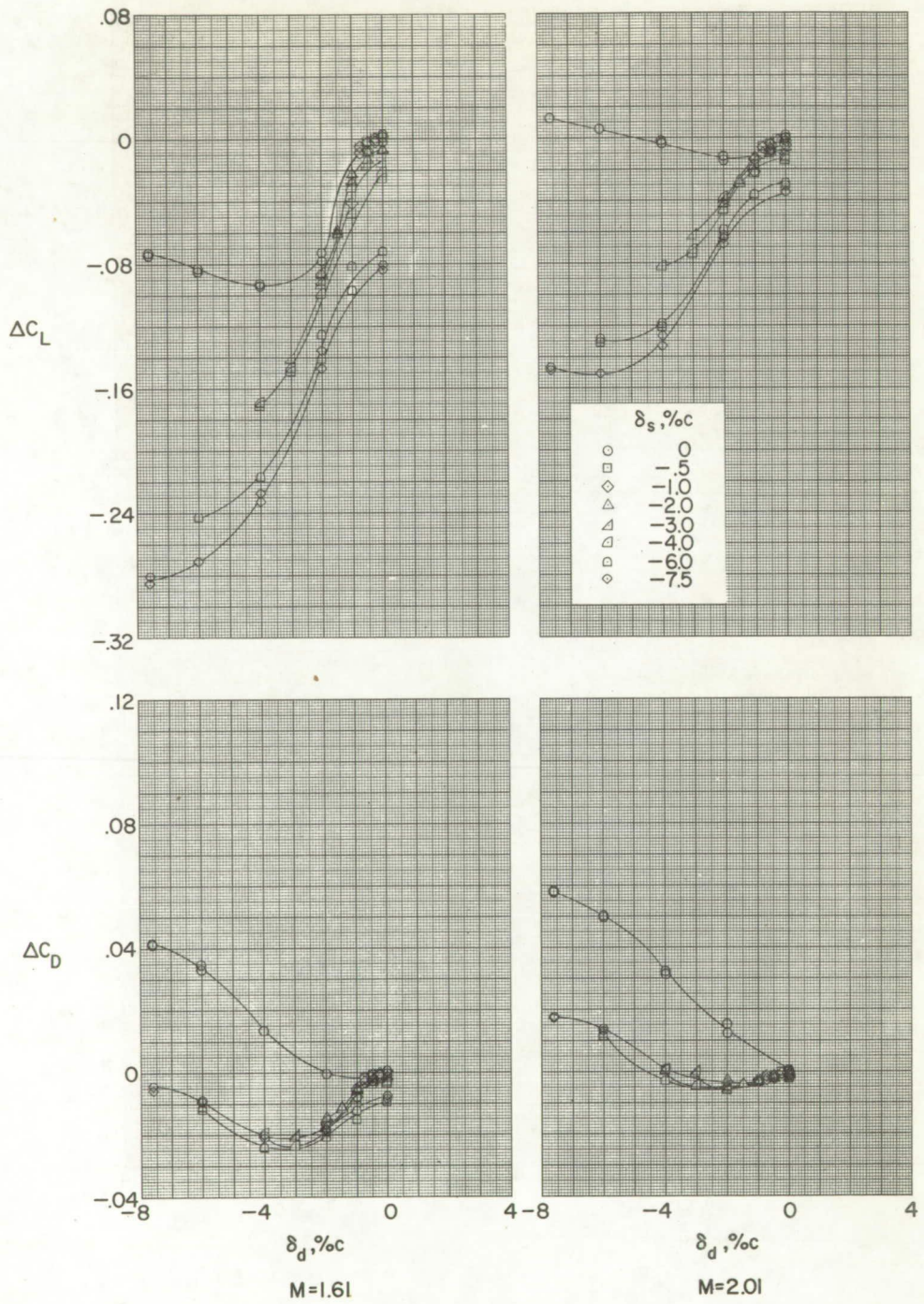

(g) $\alpha = 15^{\circ}$.

Figure 4.- Concluded.

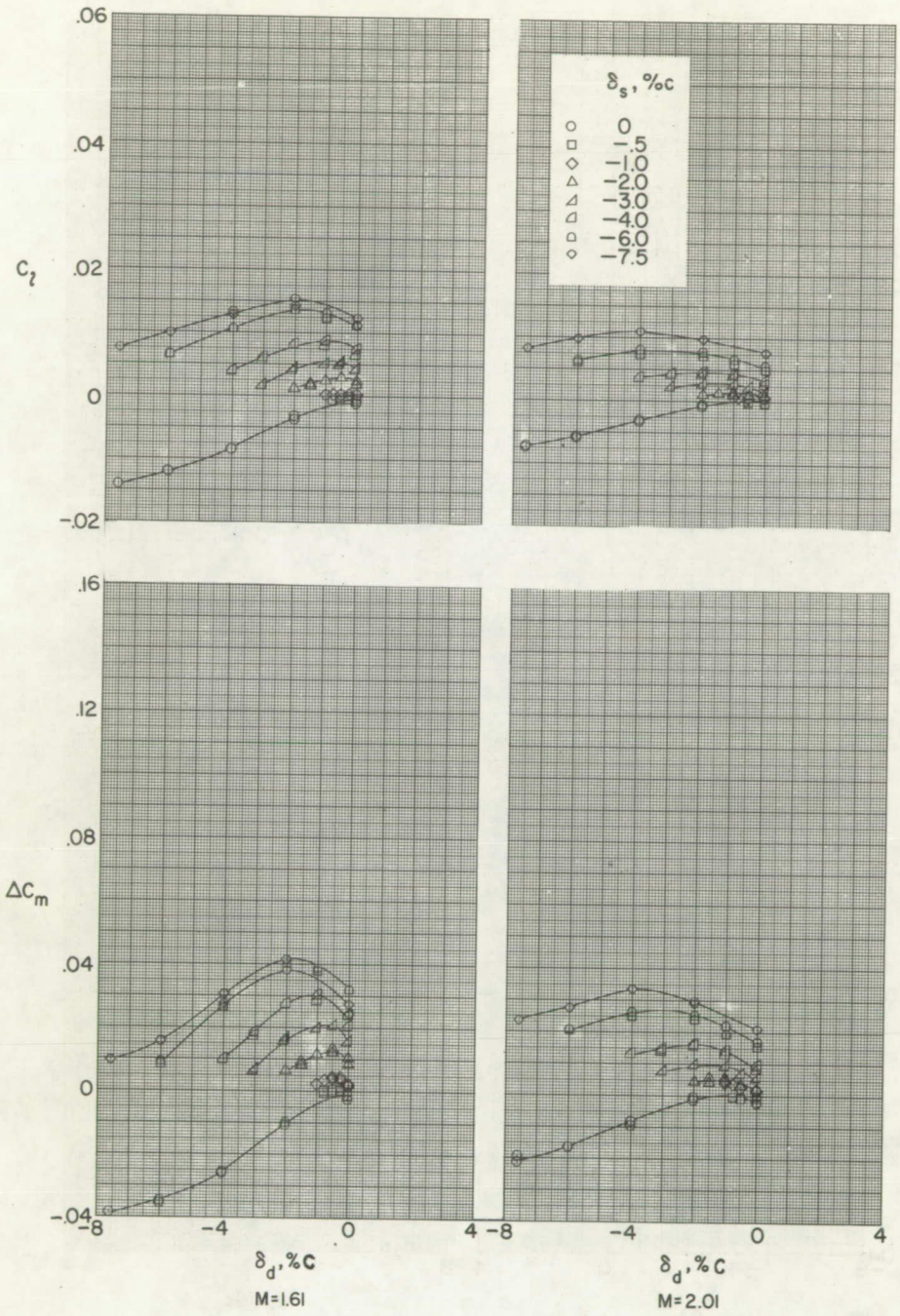

(a) $\alpha = -3^\circ$.

Figure 5.- Variation of incremental wing rolling-moment and pitching-moment coefficients with deflector projection.

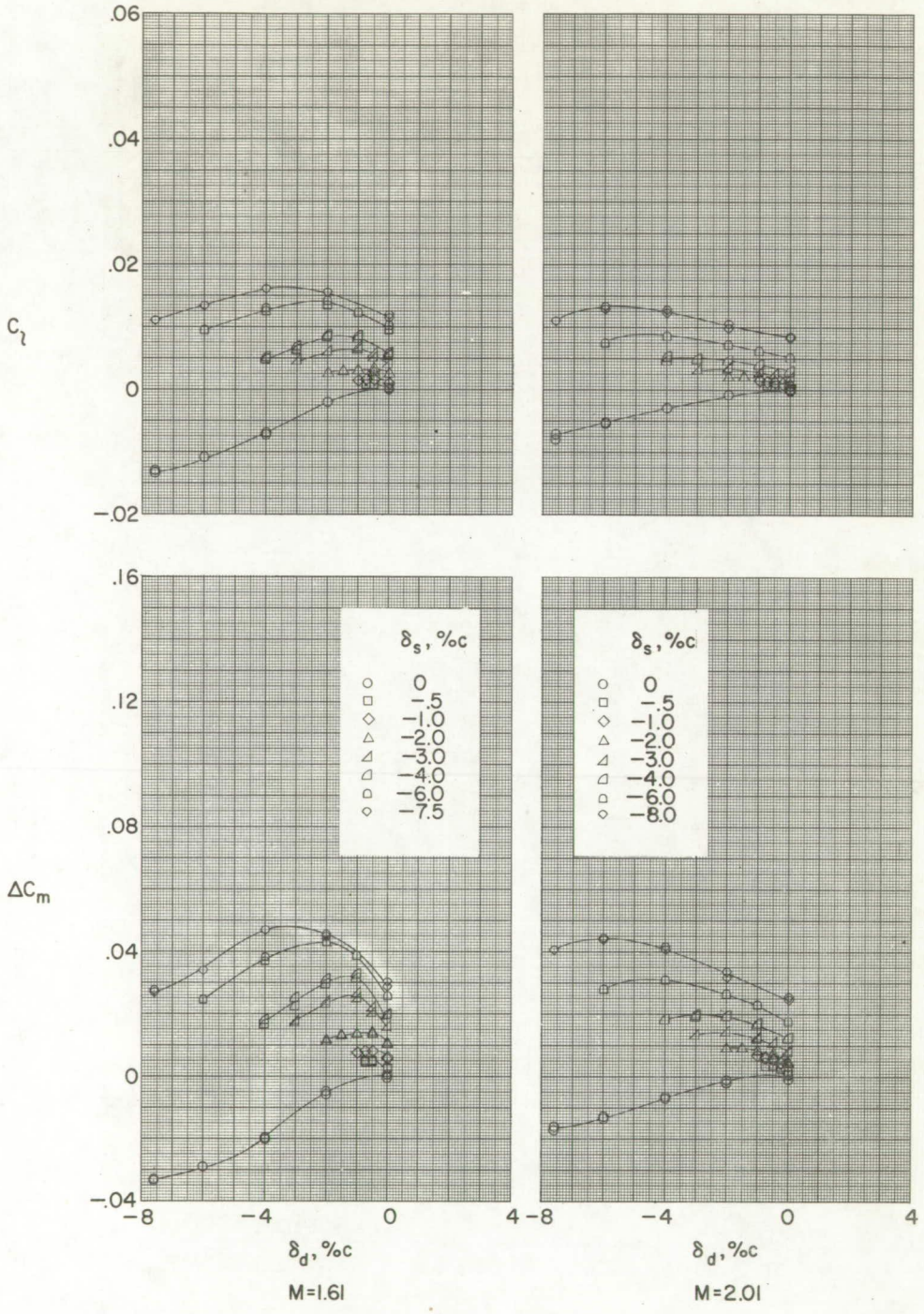

(b) $\alpha = 0^\circ$.

Figure 5.- Continued.

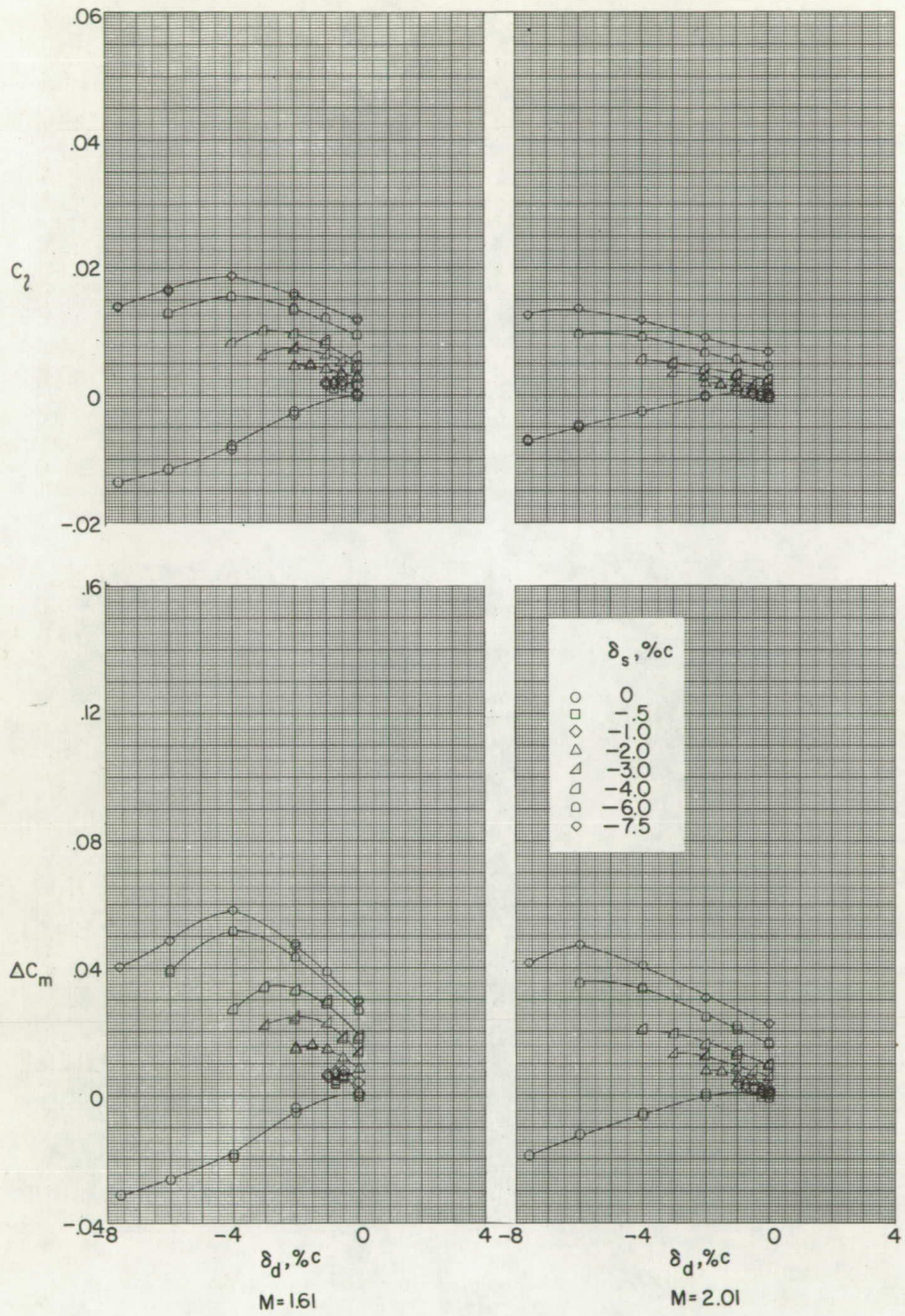

(c) $\alpha = 3^\circ$.

Figure 5.- Continued.

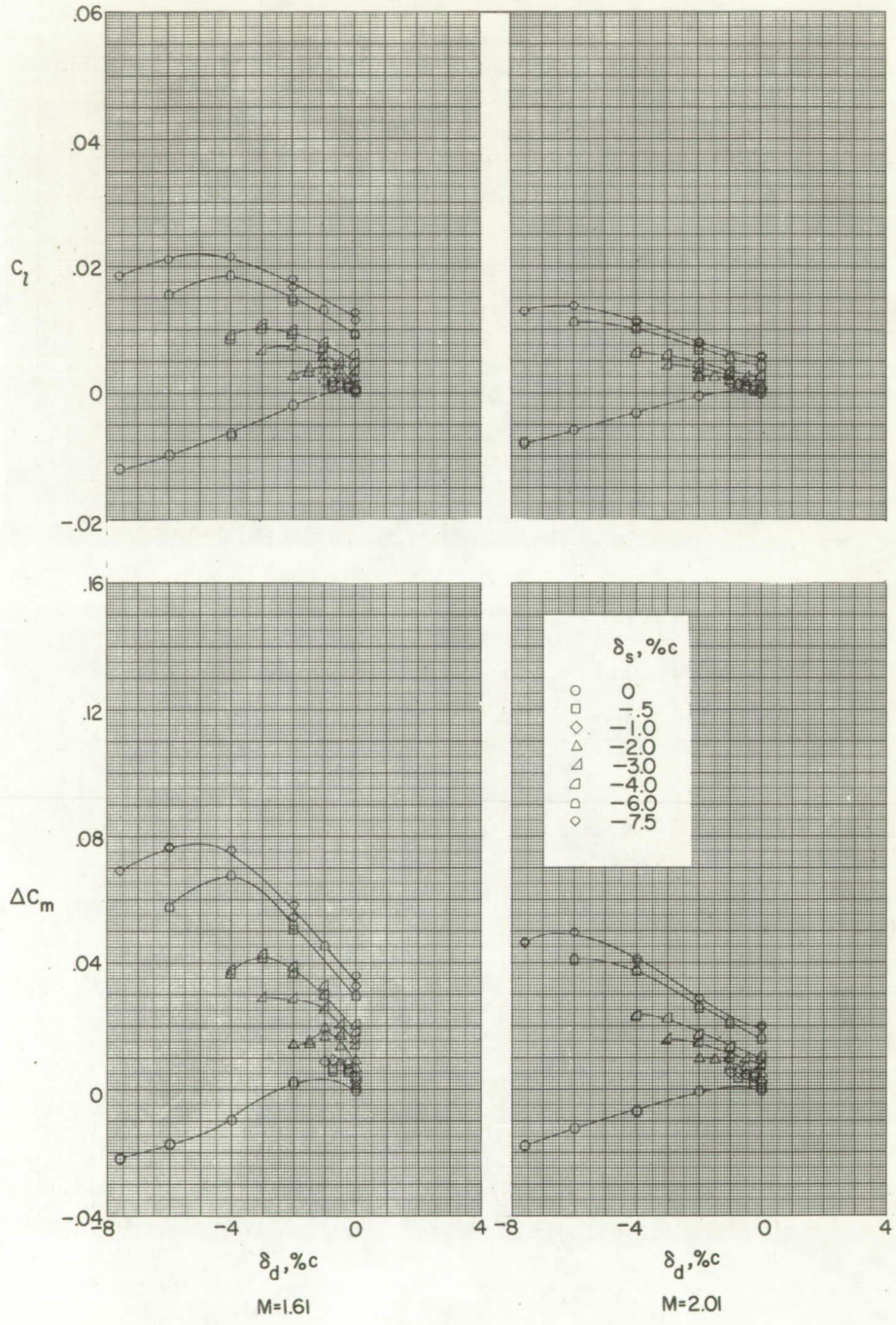

(d) $\alpha = 6^\circ$.

Figure 5.- Continued.

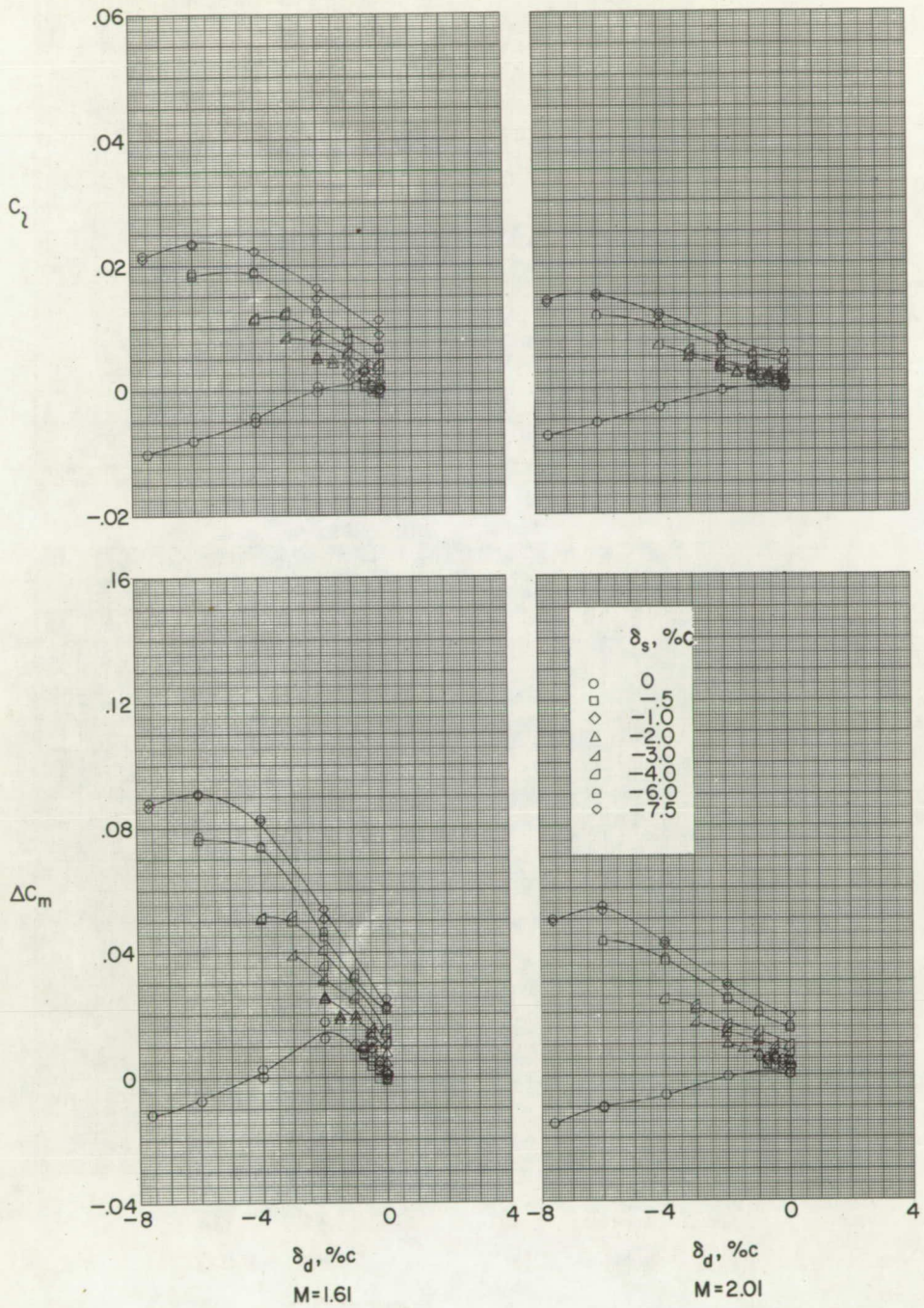

(e) $\alpha = 9^{\circ}$.

Figure 5.- Continued.

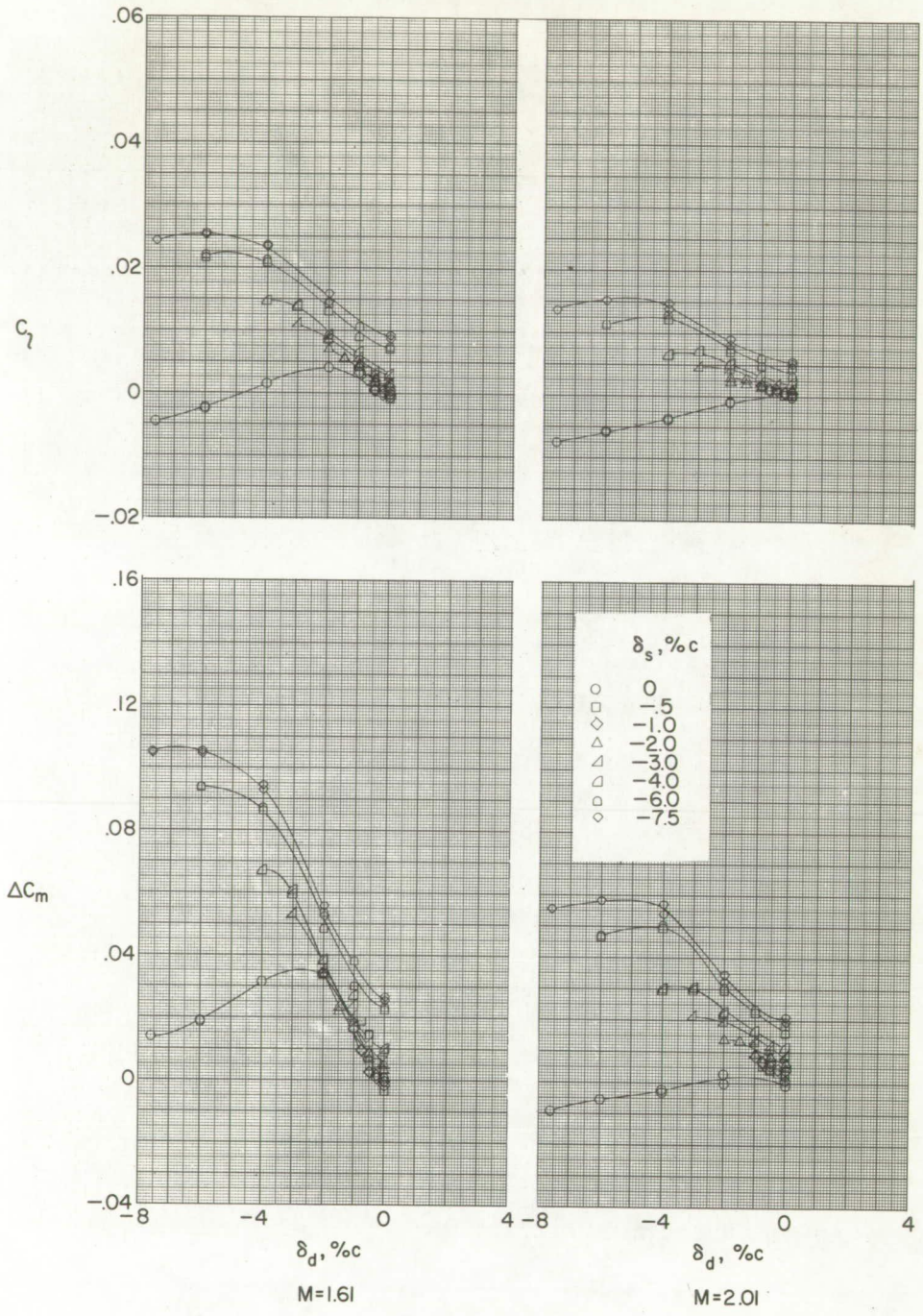

(f) $\alpha = 12^{\circ}$.

Figure 5.- Continued.

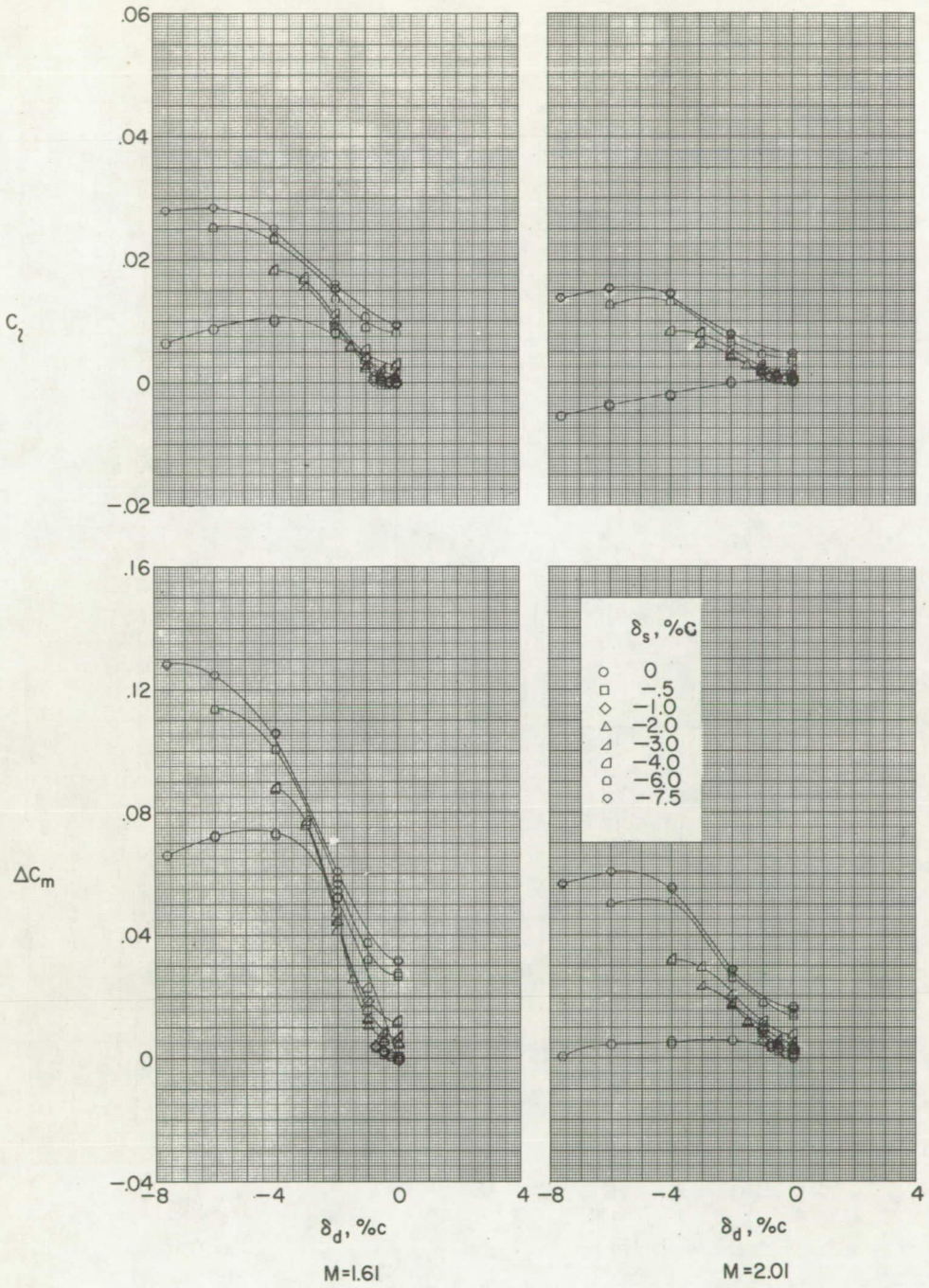

(g) $\alpha = 15^{\circ}$.

Figure 5.- Concluded.

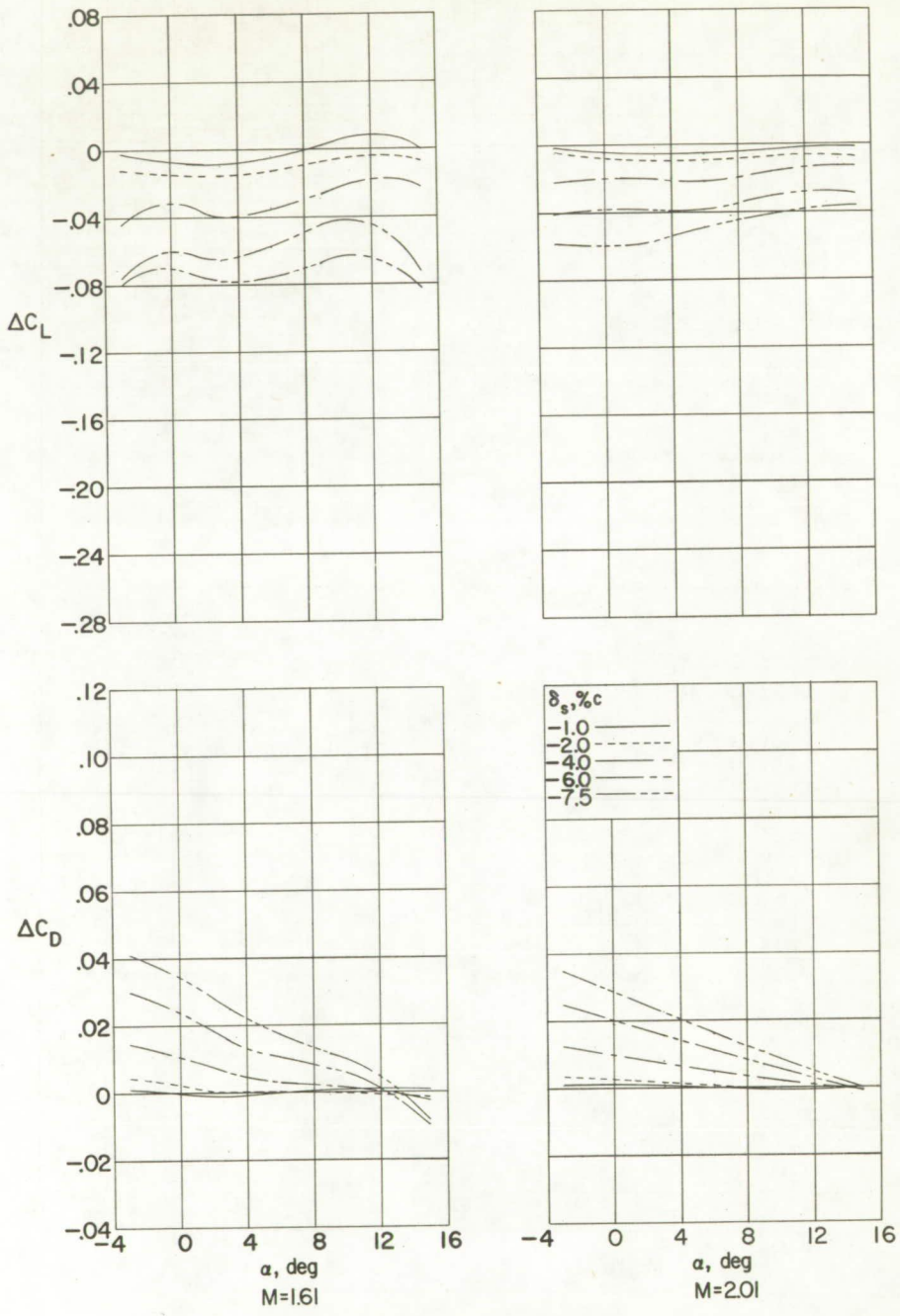

(a) $\frac{\delta_d}{\delta_s} = 0.$

Figure 6.- Variation of incremental wing lift and drag coefficients with angle of attack.

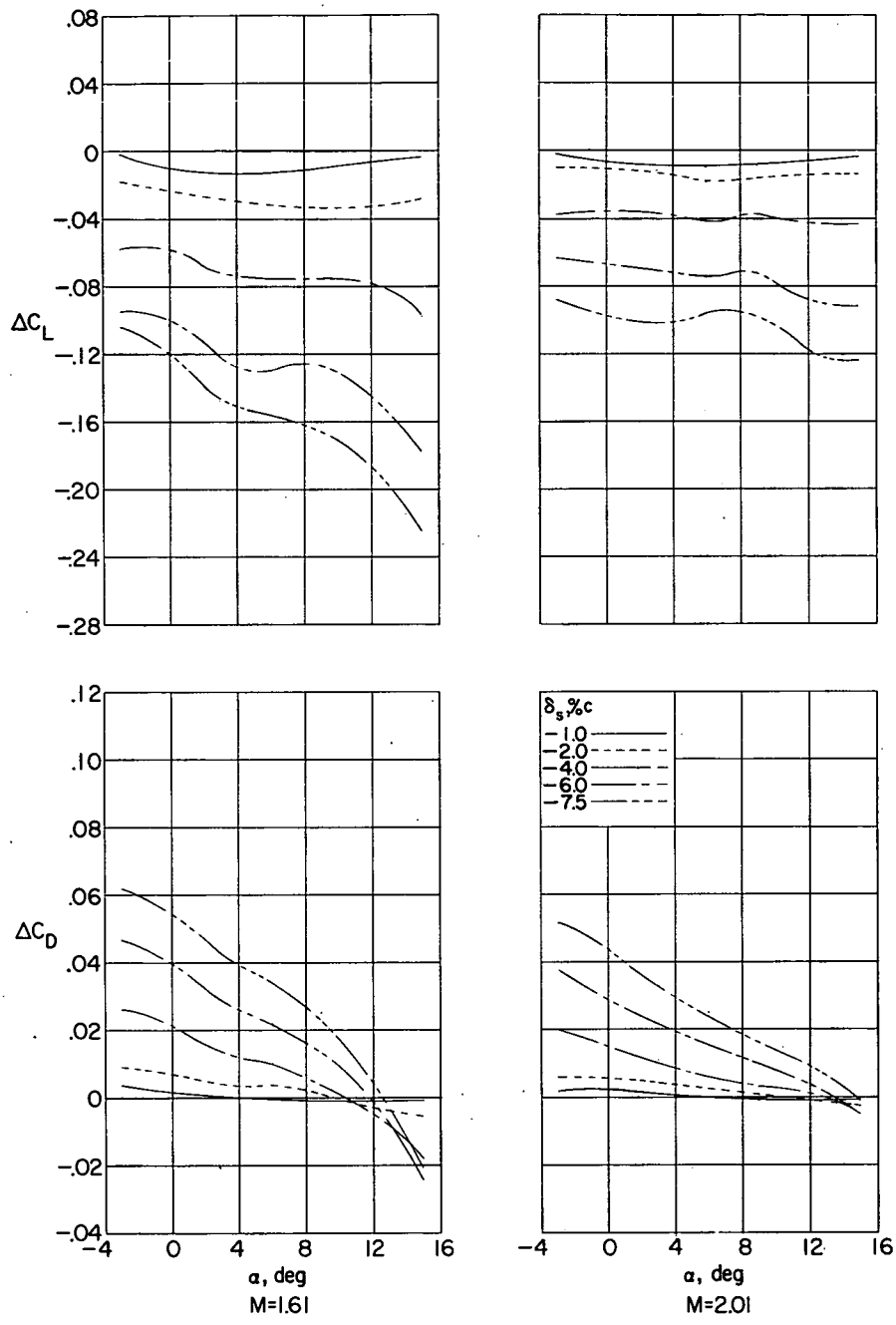

(b) $\frac{\delta_d}{\delta_s} = 0.5$.

Figure 6.- Continued.

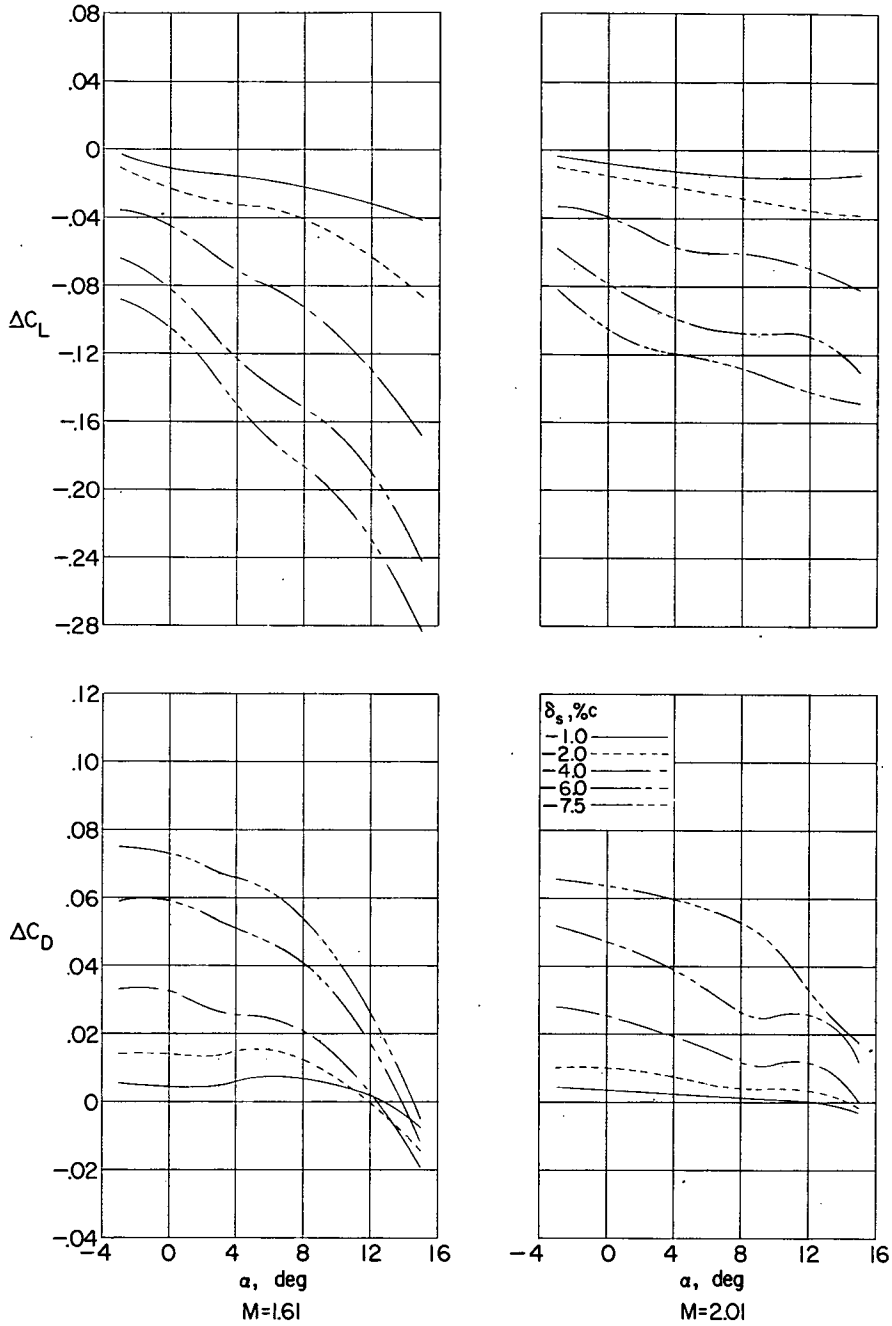

(c) $\frac{\delta_d}{\delta_s} = 1.0$.

Figure 6.- Concluded.

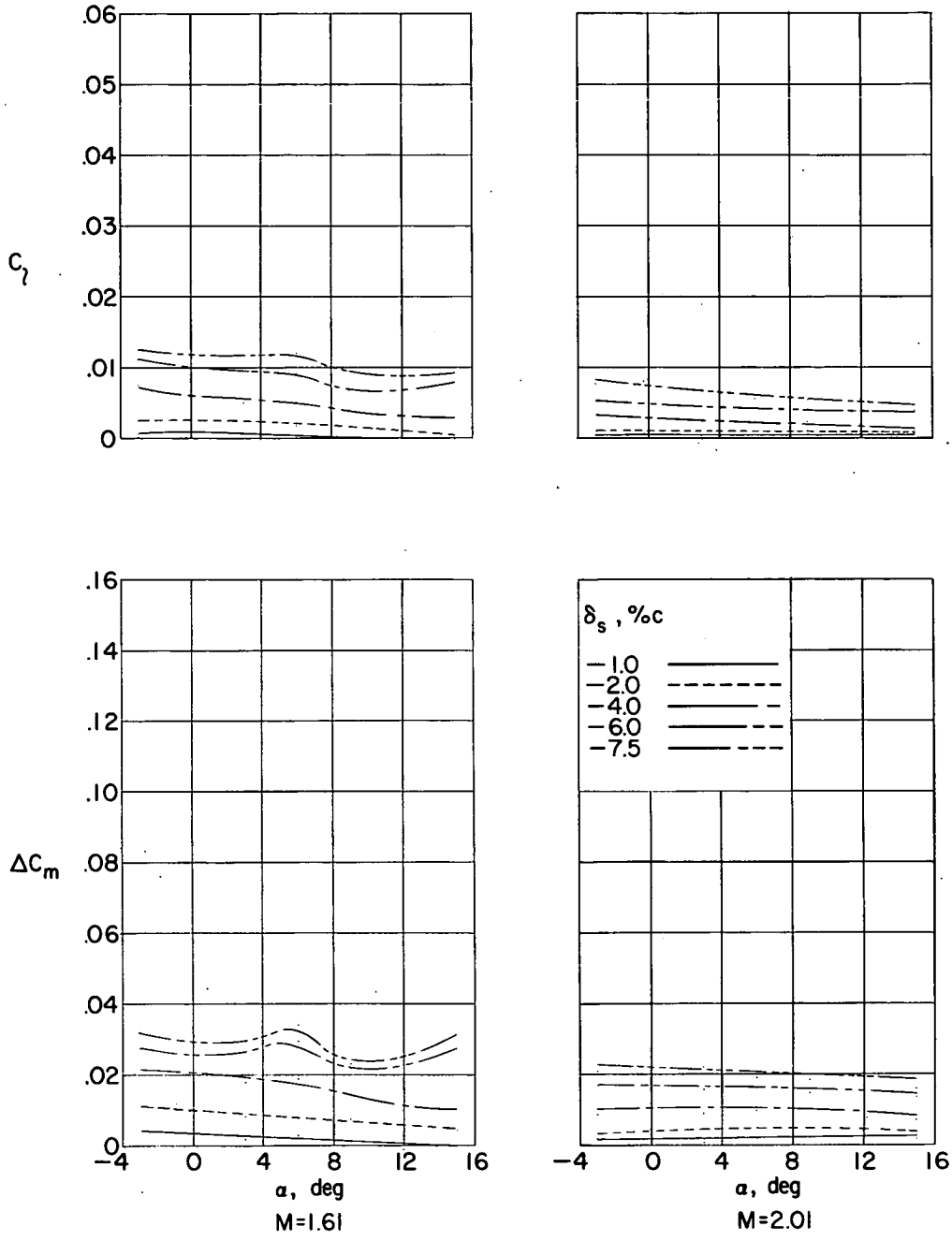

(a) $\frac{\delta_d}{\delta_s} = 0.$

Figure 7.- Variation of incremental wing rolling-moment and pitching-moment coefficients with angle of attack.

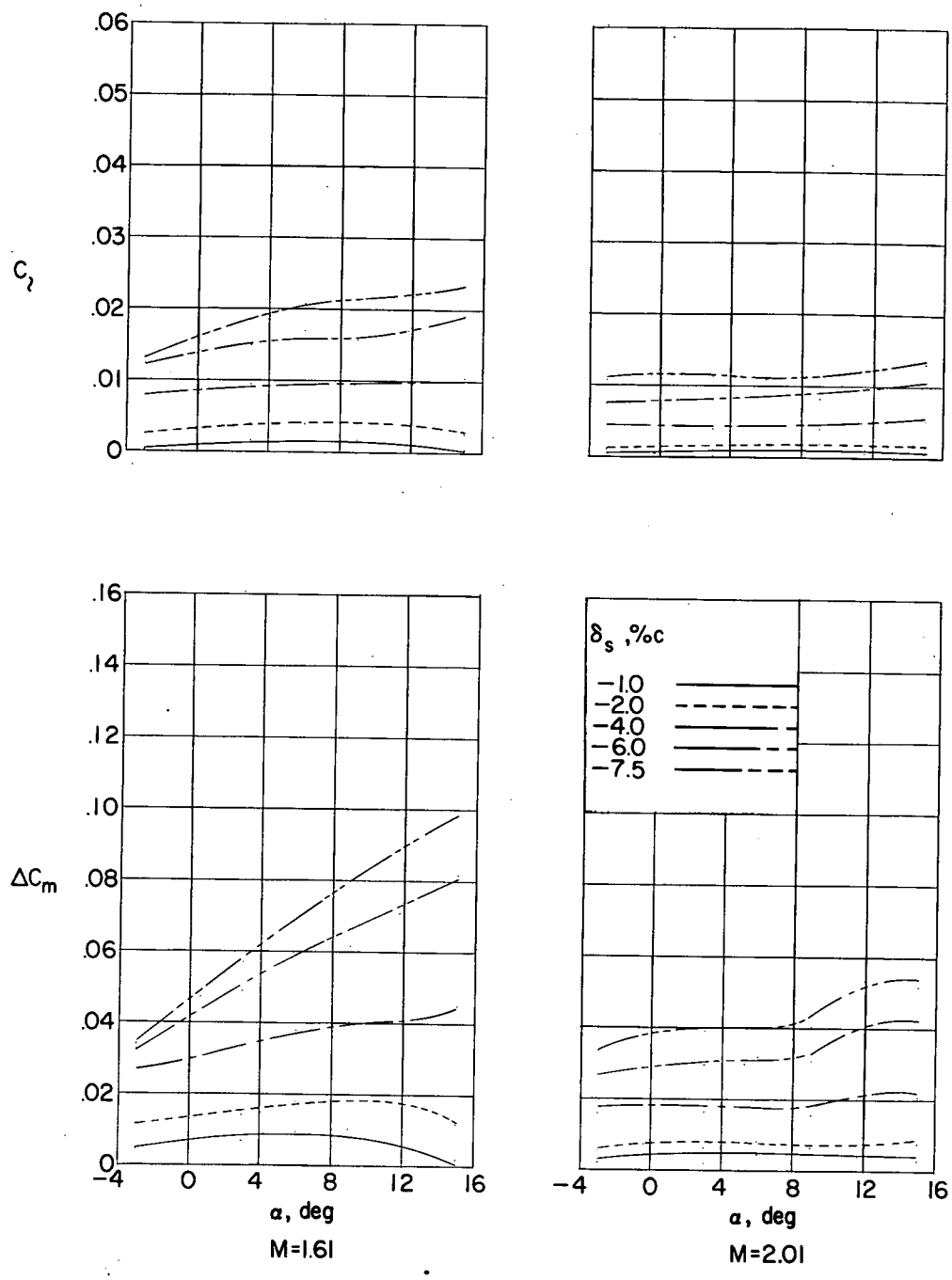

(b) $\frac{\delta_d}{\delta_s} = 0.5$.

Figure 7.- Continued.

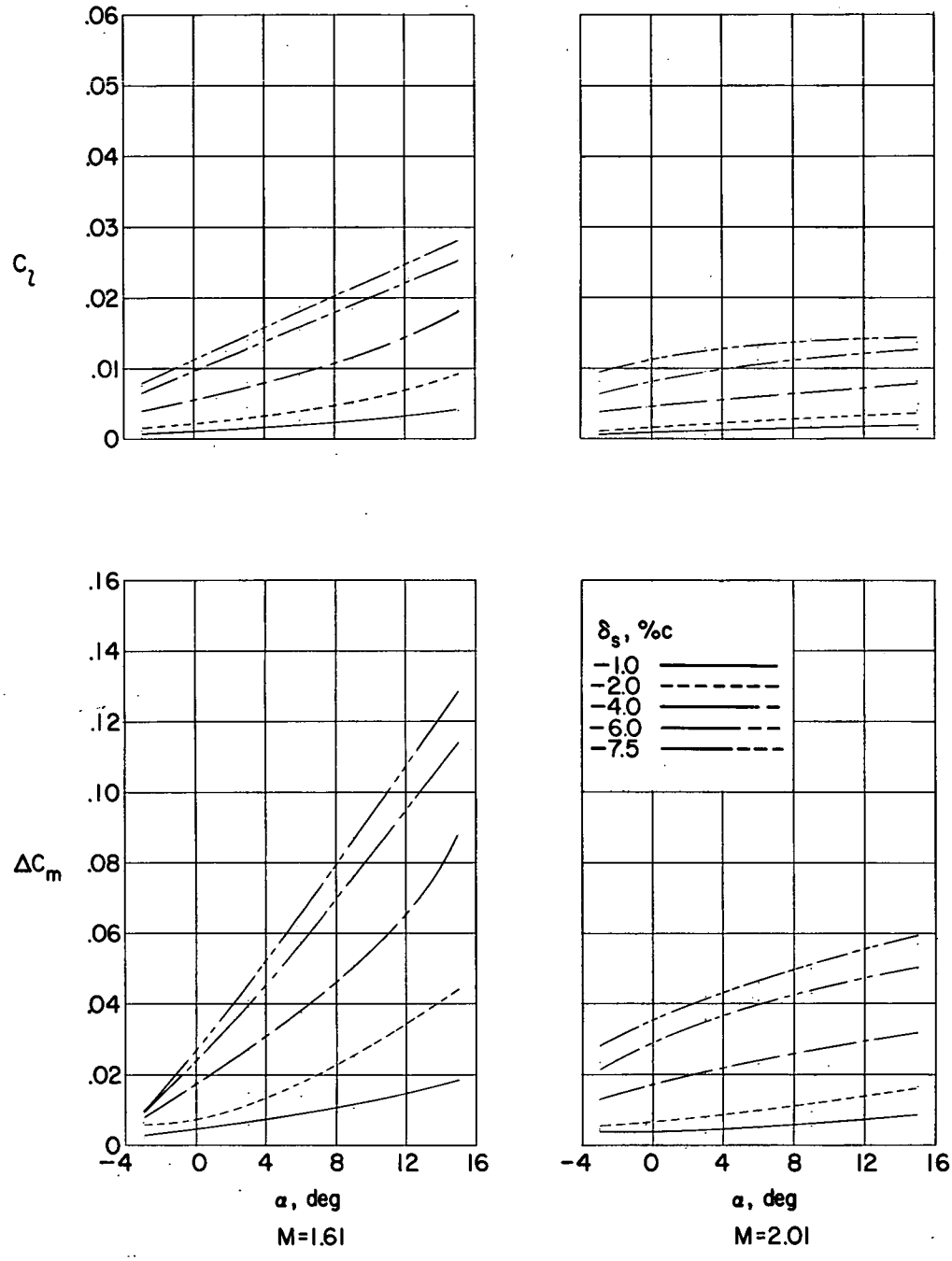

(c) $\frac{\delta_d}{\delta_s} = 1.0$.

Figure 7.- Concluded.

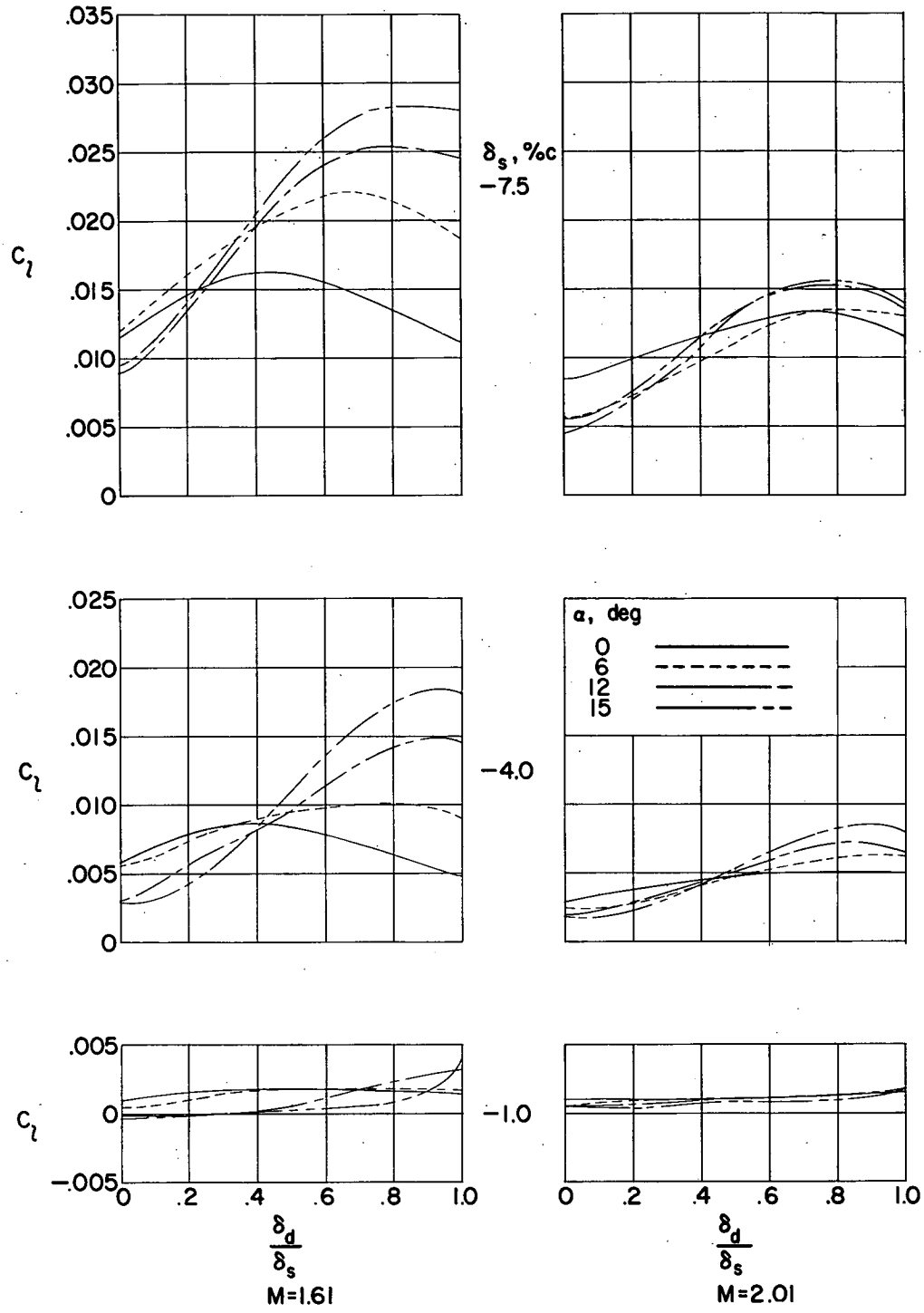

Figure 8.- Variation of wing rolling-moment coefficient with ratio of deflector projection to spoiler projection.

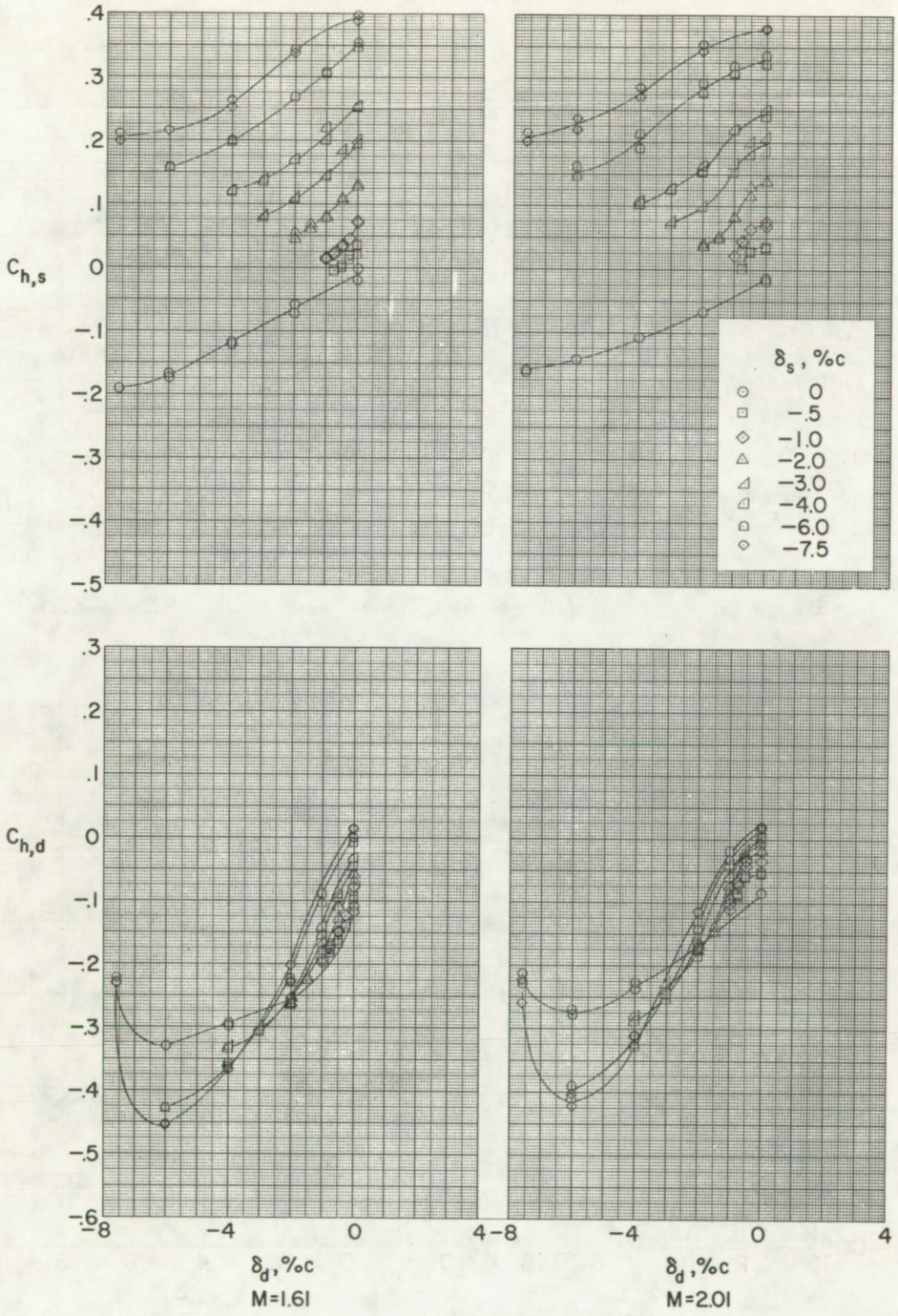

(a) $\alpha = -3^{\circ}$.

Figure 9.- Variation of spoiler and deflection hinge-moment coefficients with deflector projection.

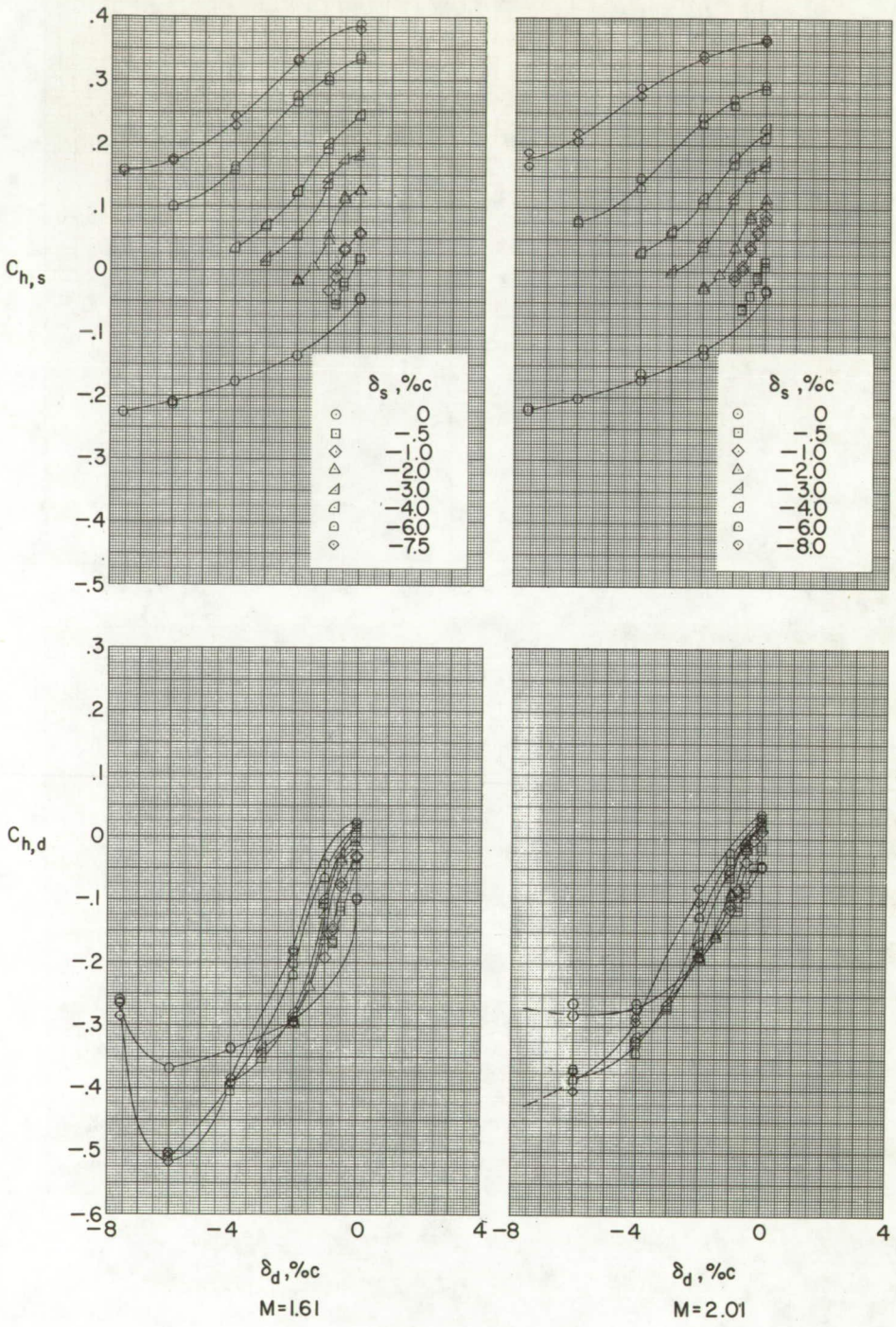

(b) $\alpha = 0^{\circ}$.

Figure 9.- Continued.

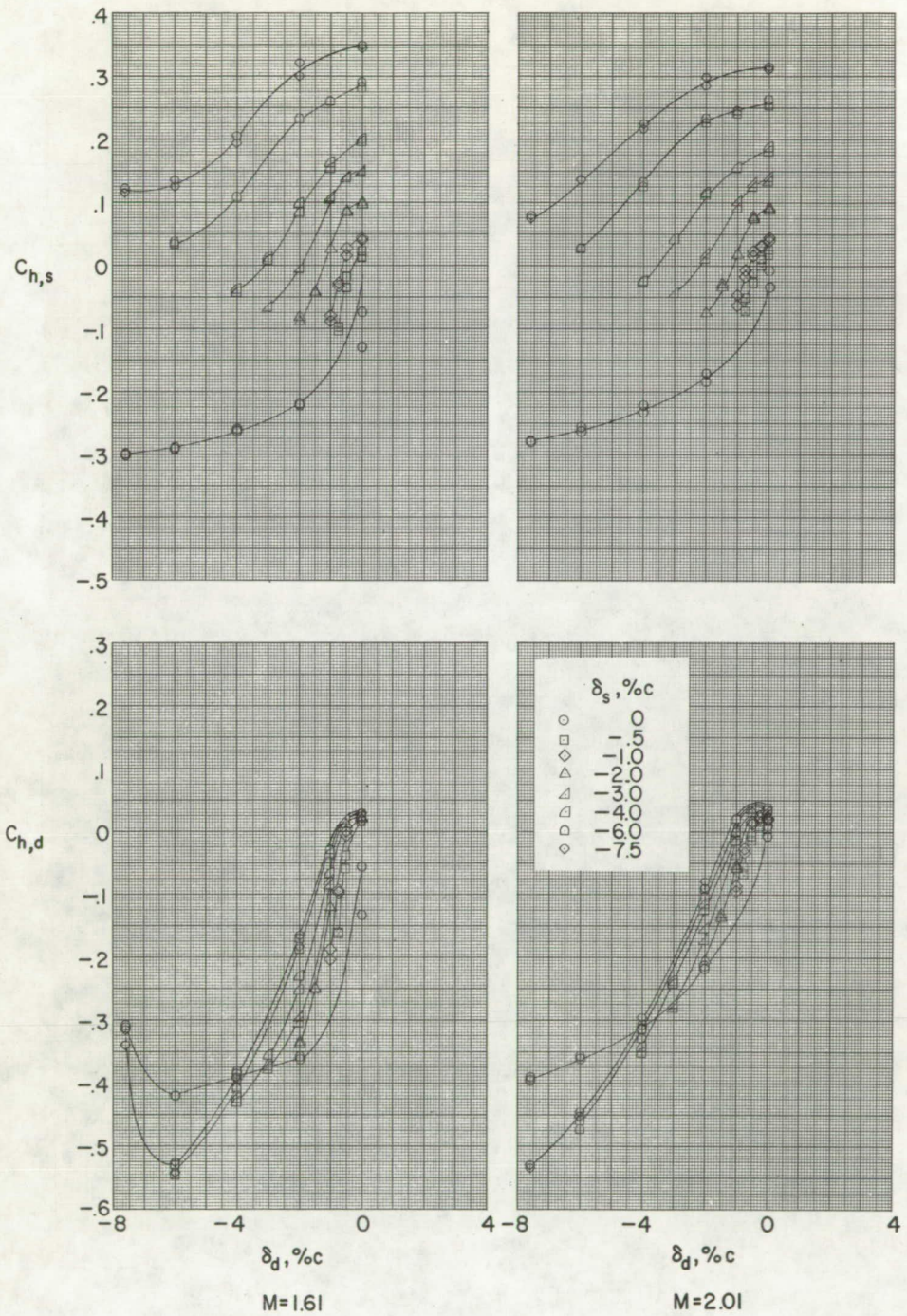

(c) $\alpha = 3^\circ$.

Figure 9.- Continued.

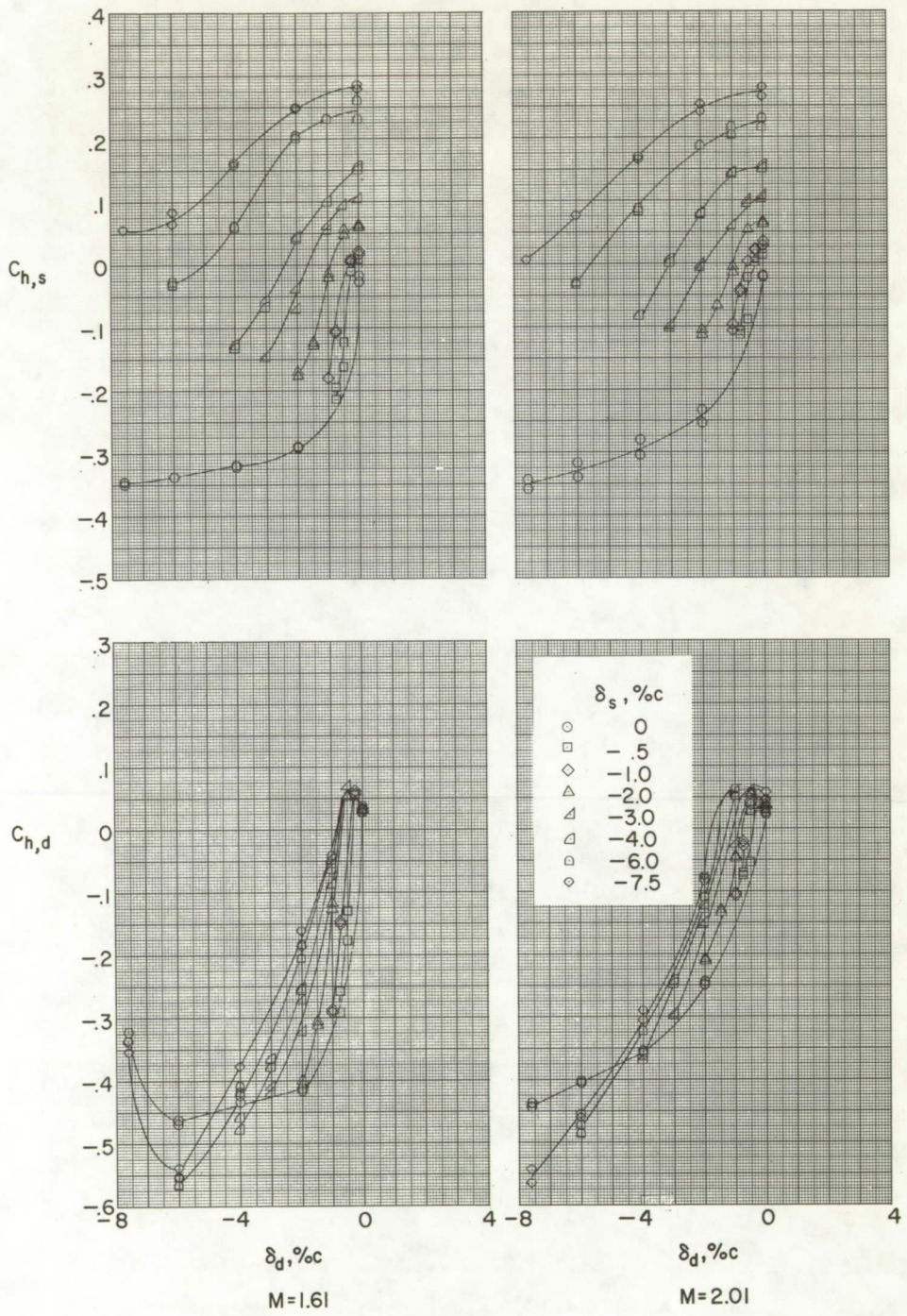

(d) $\alpha = 6^{\circ}$.

Figure 9.- Continued.

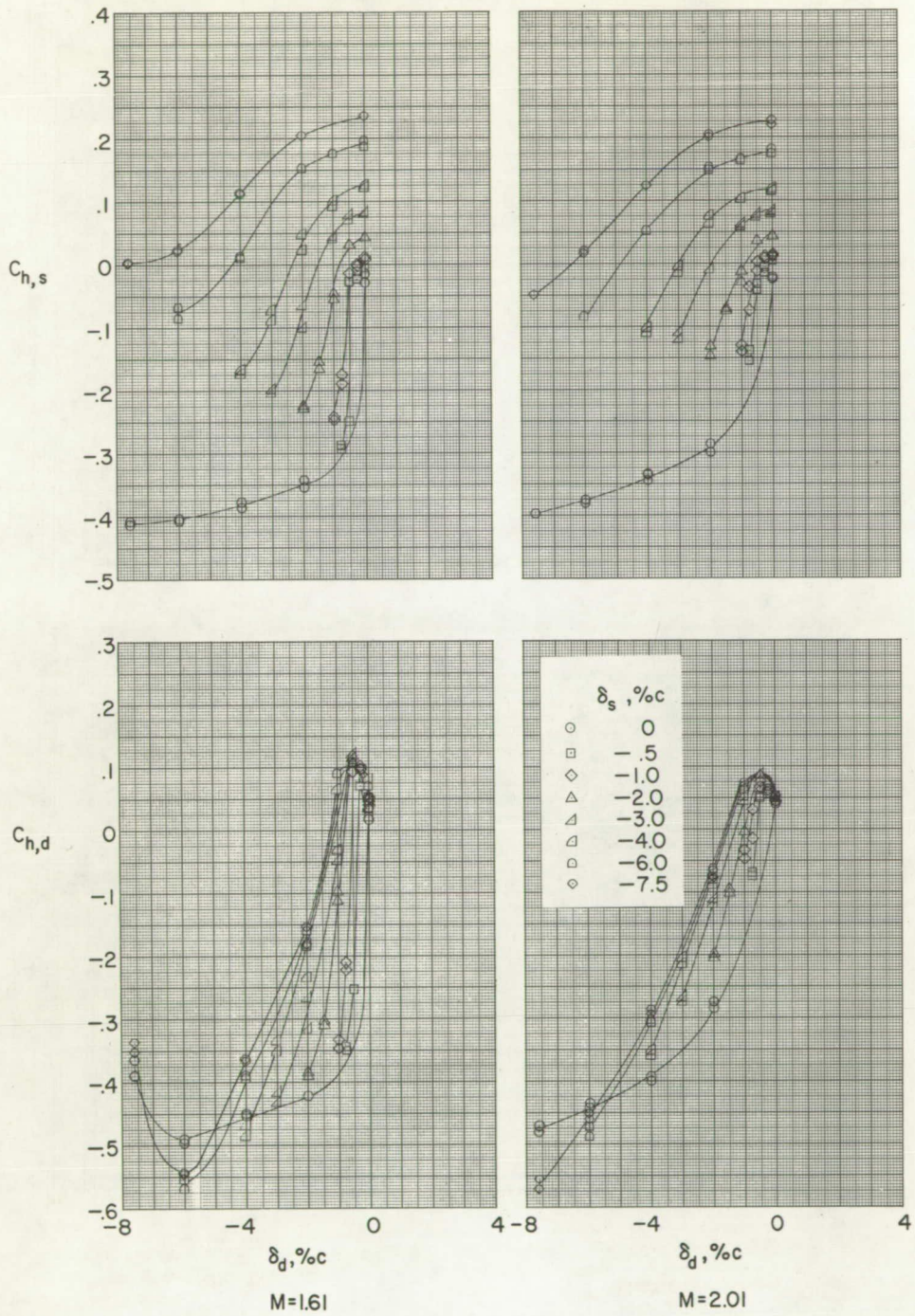

(e) $\alpha = 9^{\circ}$.

Figure 9.- Continued.

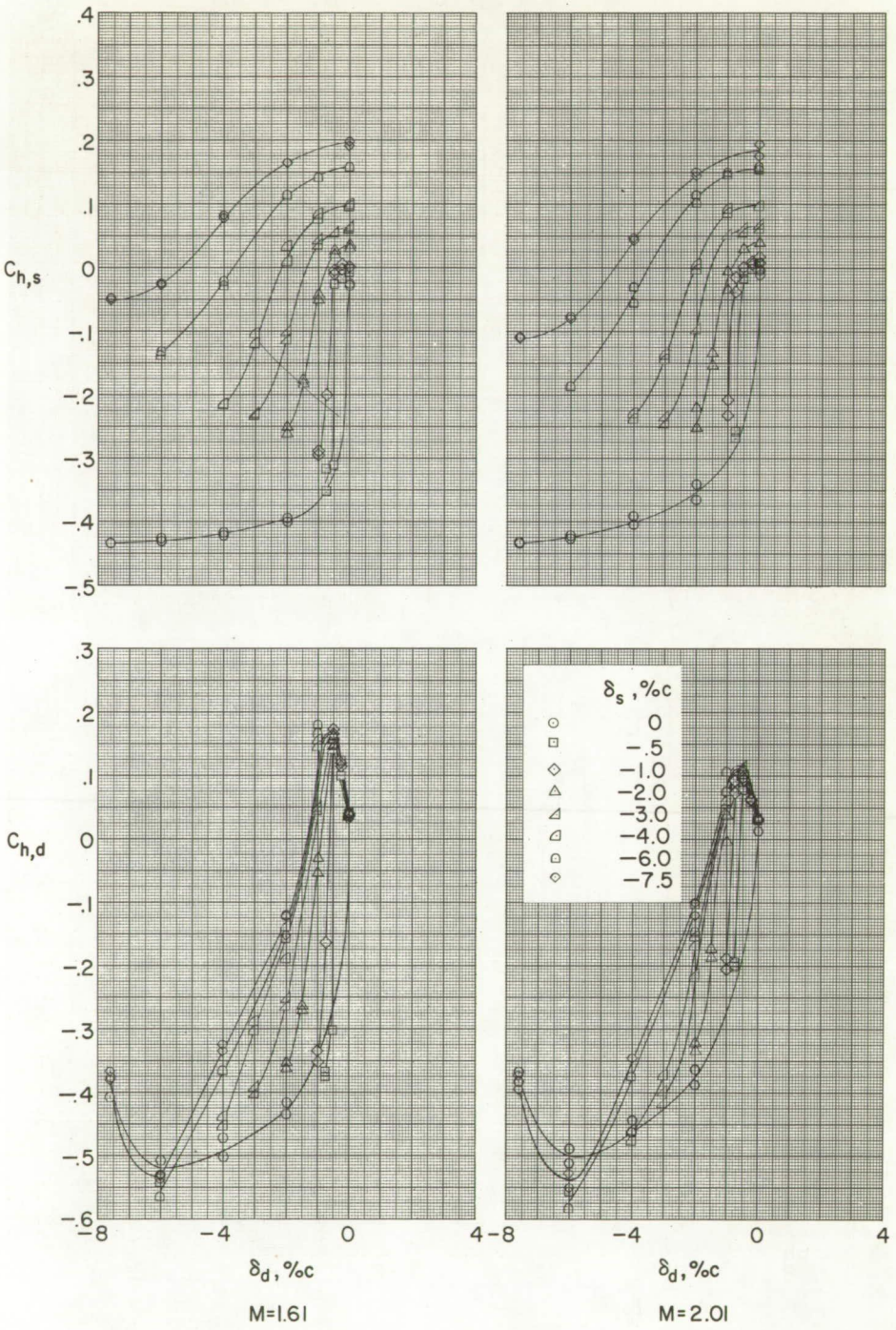

(f) $\alpha = 12^{\circ}$.

Figure 9.- Continued.

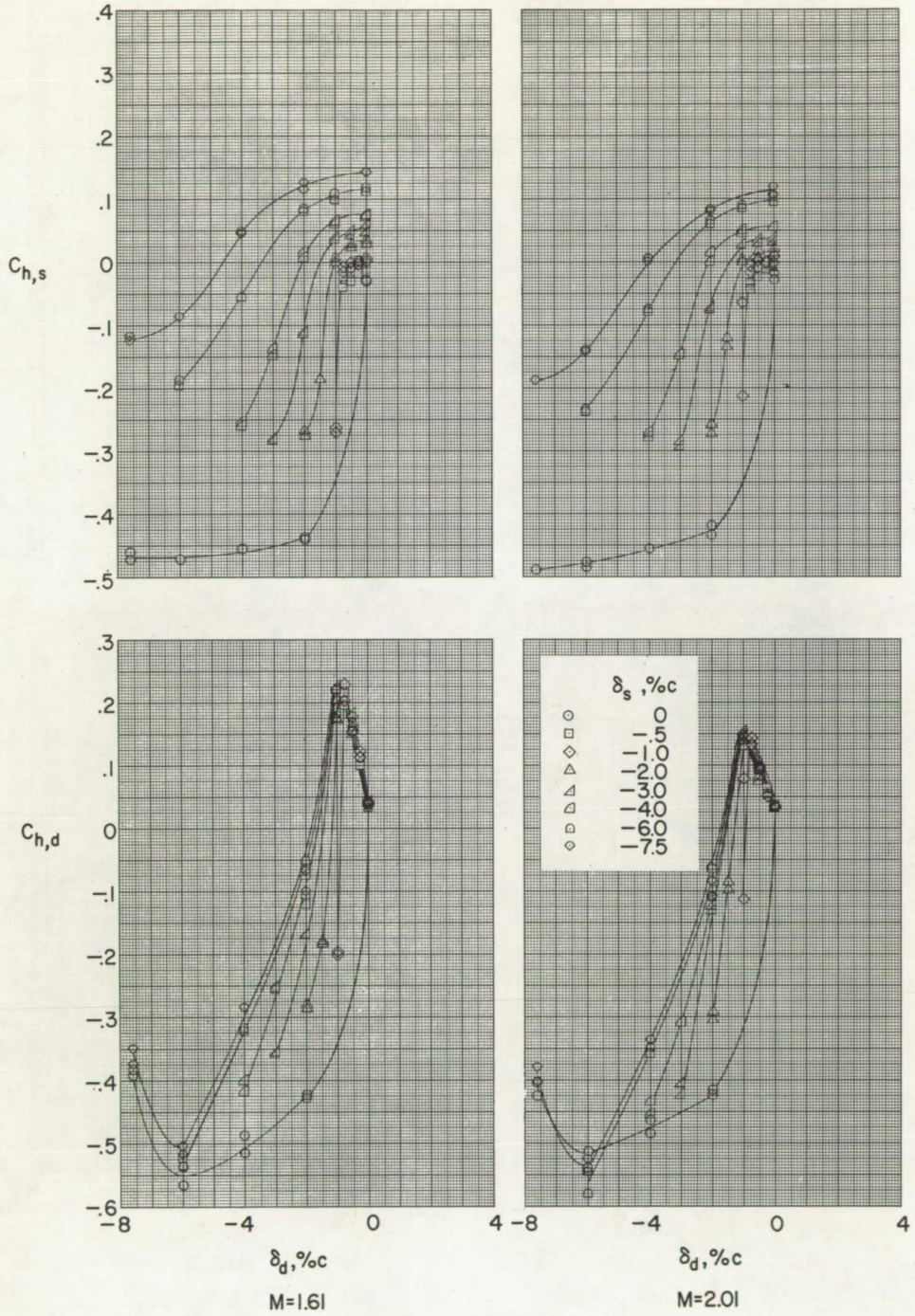

(g) $\alpha = 15^{\circ}$.

Figure 9.- Concluded.

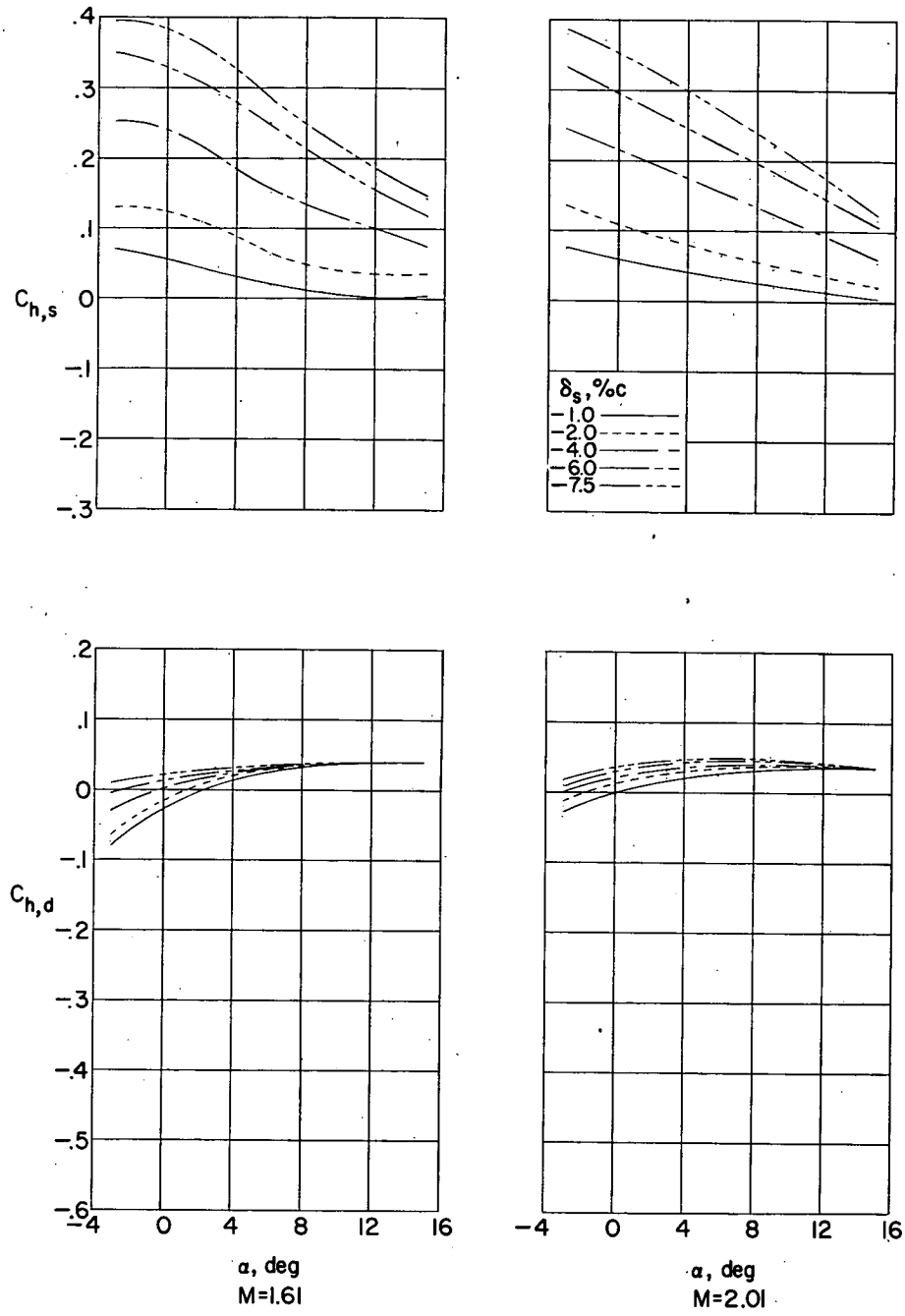

(a) $\frac{\delta_d}{\delta_s} = 0.$

Figure 10.- Variation of spoiler and deflector hinge-moment coefficients with angle of attack.

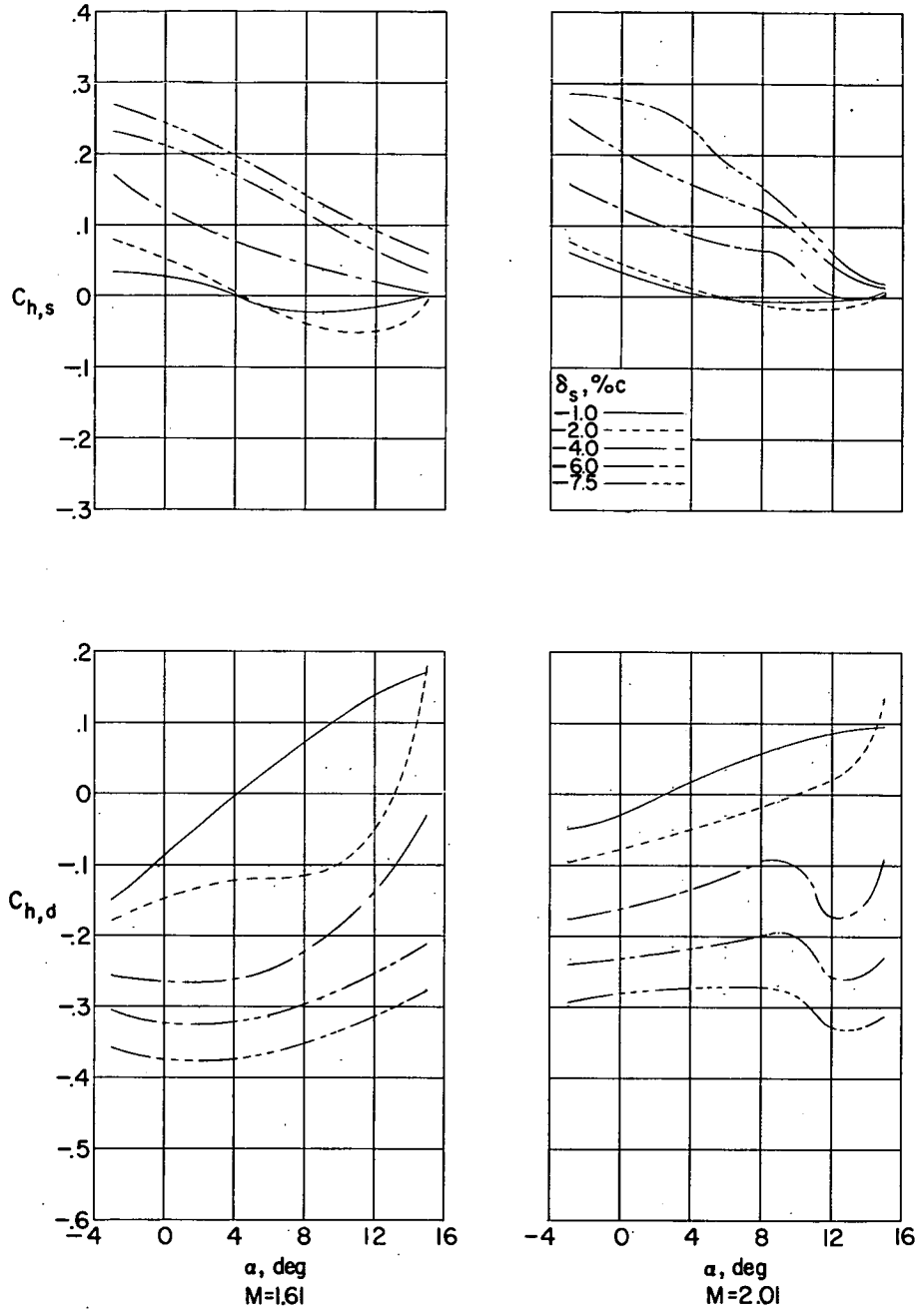

(b) $\frac{\delta_d}{\delta_s} = 0.5$.

Figure 10.- Continued.

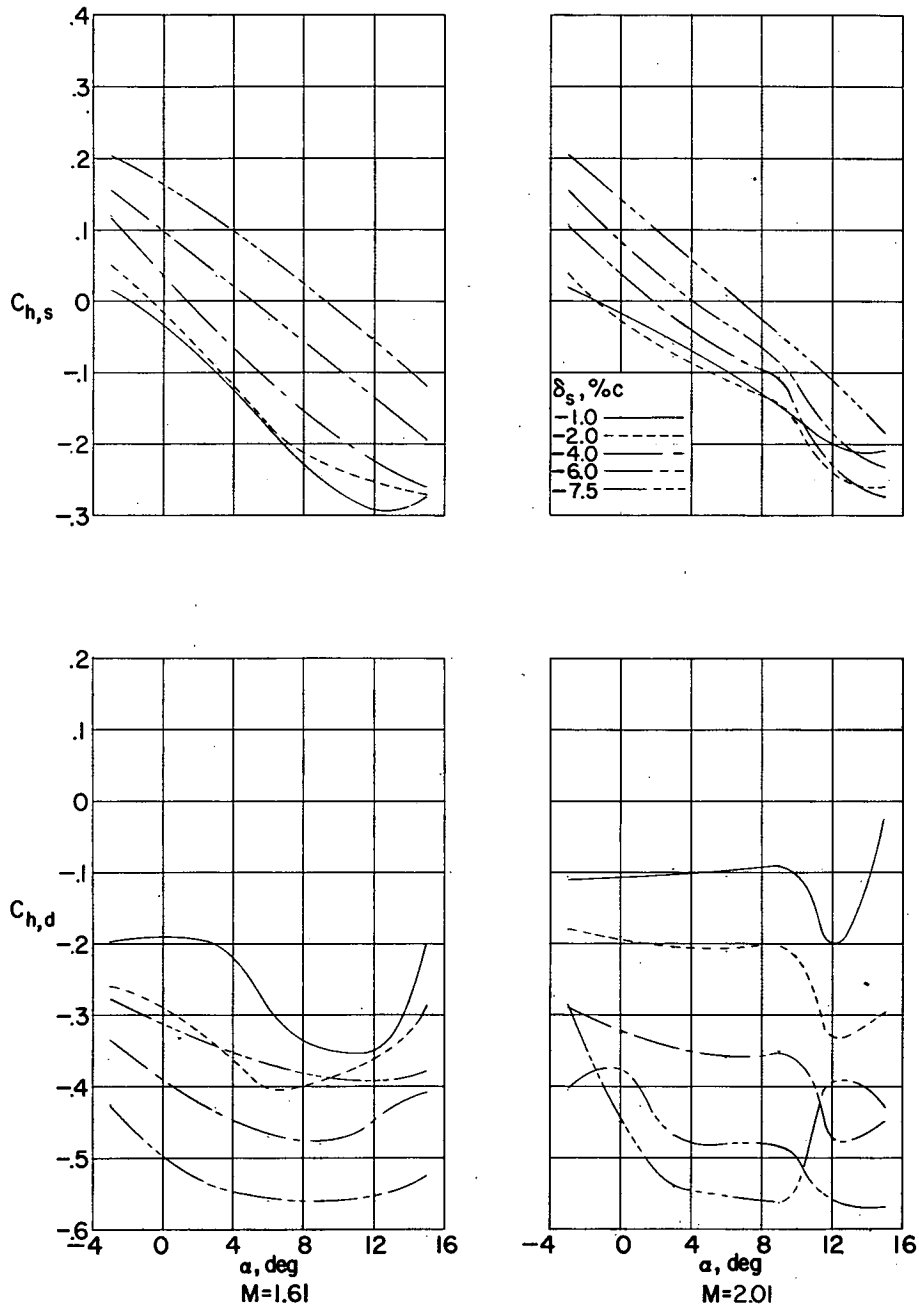

(c) $\frac{\delta_d}{\delta_s} = 1.0$.

Figure 10.- Concluded.

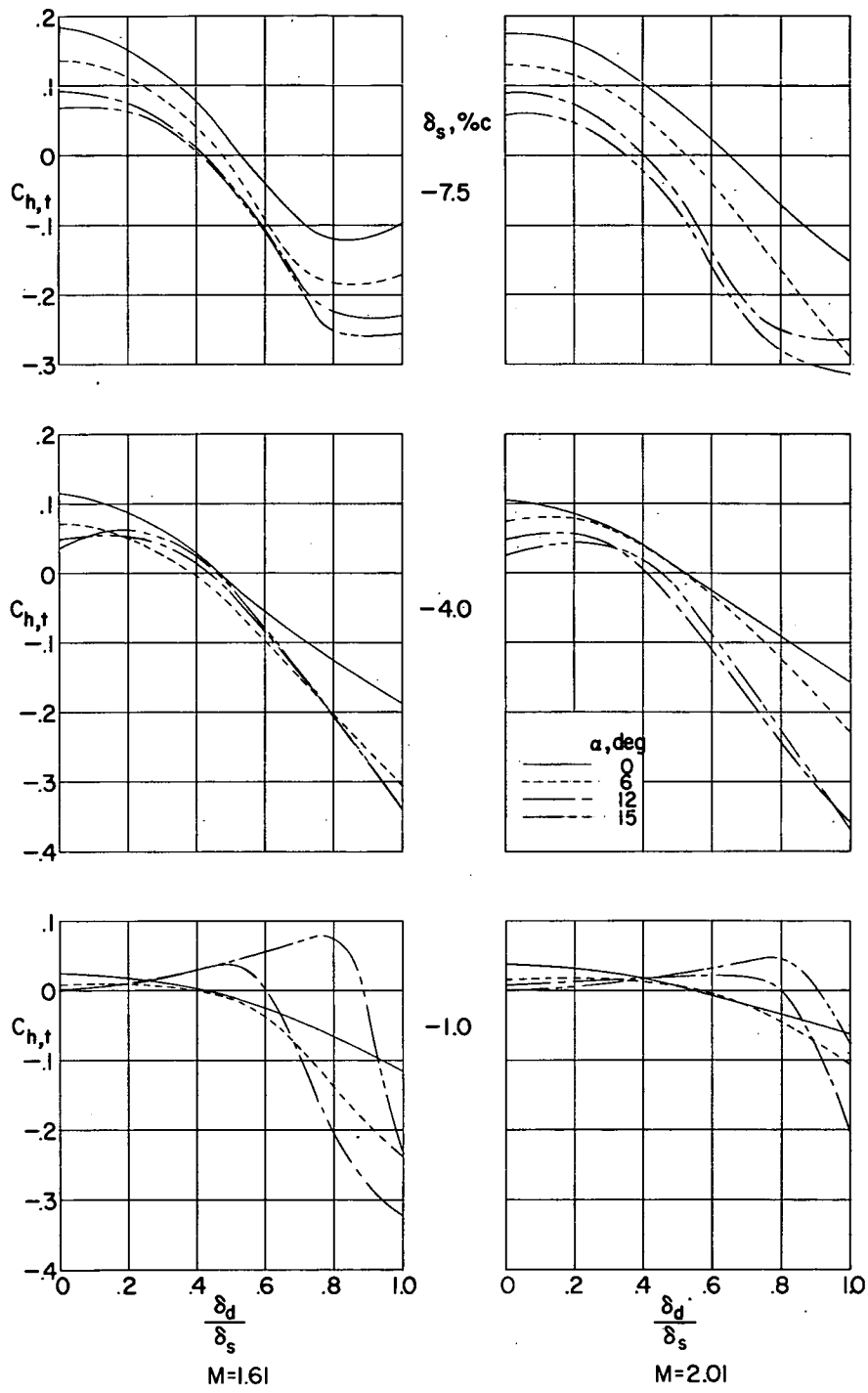

Figure 11.- Variation of the spoiler-slot-deflector total hinge-moment coefficients with ratio of deflector projection to spoiler projection.

NACA - Langley Field, Va.